# New composite bio- and isotope stratigraphies spanning the Middle Eocene Climatic Optimum at tropical ODP Site 865 in the Pacific Ocean

Kirsty M Edgar[a,b], Steven M Bohaty[c], Helen K. Coxall[d], Paul Bown[e], Sietske J. Batenburg[f], Caroline H. Lear[a] and Paul N. Pearson[a]

[a]School of Earth and Ocean Sciences, Cardiff University, Cardiff, CF10 3AT, UK

[b]School of Geography, Earth and Environmental Sciences, University of Birmingham, B15 2TT, UK

[c]Ocean and Earth Science, National Oceanography Centre Southampton, University of Southampton, SO14 3ZH, UK

[d]Department of Geological Sciences, Stockholm University, SE-106 91, Stockholm Sweden

[e]Department of Earth Sciences, University College London, London, WC1E 6BT, UK

[f]University of Rennes, CNRS, Géosciences Rennes, UMR 6118, 35000 Rennes, France

**Corresponding author**

Kirsty M Edgar - E: k.m.edgar@bham.ac.uk. T: +44 (0) 121 414 6163. School of Geography, Earth and Environmental Sciences, Aston Webb Block A, University of Birmingham, Edgbaston, B15 2TT, UK

**Abstract**

The Middle Eocene Climatic Optimum (MECO) at ca. 40 Ma is one of the largest of the transient Eocene global warming events. However, it is relatively poorly known from tropical settings as few sites span the entirety of the MECO event and/or host calcareous microfossils, which are the dominant proxy carrier. Ocean Drilling Program (ODP)

Pacific Ocean Site 865 in the low-latitude North Pacific (Allison Guyot) has the potential to provide a useful tropical MECO reference but detailed stratigraphic and chronological constraints needed to evaluate its completeness were previously lacking. We have addressed this deficit by generating new high-resolution biostratigraphic, stable isotope and X-ray fluorescence (XRF) records spanning the MECO interval (~38.0–43.0 Ma) in two holes drilled at Site 865. XRF records of Sr/Ca, Ba/Sr and Fe allow correlation between holes and reveal pronounced rhythmicity, enabling us to develop the first composite section for Holes 865B and 865C and a preliminary cyclostratigraphy for the MECO. Using this new framework, the sedimentary record is interpreted to be continuous across the event, as identified by a pronounced transient $\delta^{18}O$ shift of ~0.8‰. Calcareous microfossil biostratigraphic events from widely used zonation schemes are recognized, with generally good agreement between the two holes, highlighting the robustness of the new composite section and allowing us to identify planktic foraminiferal Zones E10-E15 and calcareous nannofossil Zones NP15–18. However, discrepancies in the relative position and ordering of several primary and secondary bioevents with respect to published schemes are noted. Specifically, the stratigraphic highest occurrences of planktic foraminifera *Acarinina bullbrooki, Guembelitrioides nuttalli*, and *Morozovella aragonensis,* and calcareous nannofossils *Chiasmolithus solitus* and *Sphenolithus furcatolithoides* and the lowest occurrence of *Cribrocentrum reticulatum,* all appear higher in the section than would be predicted relative to other bioevents. We also note conspicuous reworking of older microfossils (from planktic foraminiferal Zones E5-E9 and E13) into younger sediments (planktic foraminiferal Zones E14-15) within our study interval consistent with reworking in the topmost ~30 m of the site. Regardless of reworking, the high-quality, XRF records enable decimeter scale correlation between holes and highlight the potential of Site 865 for constraining tropical environmental and biotic changes, not just across the MECO but also throughout the Paleocene and early-middle Eocene.

**Keywords**

MECO, planktic foraminifera, biostratigraphy, XRF, benthic isotope stratigraphy

## Introduction

The transition from peak Eocene 'greenhouse' conditions at ~50–52 Ma to the onset of the icehouse at ~34 Ma is punctuated by a number of transient climate events (e.g., Bohaty et al., 2009; Edgar et al., 2007; Sexton et al., 2011; Zachos et al., 2008). The most pronounced of these is the MECO event at ~40 Ma that represents a temporary reversal in the long-term Eocene global cooling trend (Bohaty and Zachos, 2003; Bohaty et al., 2009). The MECO event is characterized by ocean warming of ~3–6˚C (Bijl et al., 2010; Bohaty et al., 2009; Boscolo Galazzo et al., 2014; Edgar et al., 2010), ocean acidification evidenced by >1 km shoaling of the Pacific calcite compensation depth (CCD), and shifts in the global carbon cycle (Bohaty et al., 2009; Pälike et al., 2012). Biotic responses vary across the event, impacting floral and faunal composition, body size, and ecology in the deep and surface ocean globally (e.g., Arreguín-Rodríguez et al., 2016a; Boscolo Galazzo et al., 2015; Cramwinckel et al., 2019; Edgar et al., 2013; Luciani et al., 2010; Möbius et al., 2015; Witkowski et al., 2014).

The MECO is well known from mid- and high-latitude sites (e.g., ODP Sites 689, 690, 702, 748, 738, 1051, 1172 and 1263 and the Alano, Contessa Highway and Monte Cagnero sections in Italy), many of which also are characterized by good stratigraphic age control, comprehensive isotope stratigraphies and carbonate rich sediments yielding microfossil useful for proxy reconstructions (Bijl et al., 2010; Bohaty and Zachos, 2003; Bohaty et al., 2009; Boscolo Galazzo et al., 2014; Edgar et al., 2010; Jovane et al., 2007; Rivero-Cuesta et al., 2019; Savian et al., 2013; Spofforth et al., 2010). However, we currently lack a low-latitude site that unambiguously spans the pre-MECO, MECO and

post-MECO intervals and has continuous carbonate sedimentation uninterrupted by CCD or lysocline shoaling, thus hindering our understanding of environmental and biotic responses in the tropics.

Of the sites that do exist, ODP Site 1260 in the equatorial Atlantic has a high-resolution stable isotope stratigraphy that has been placed onto an orbitally tuned age model providing unprecedented age control (Edgar et al., 2010; Westerhold and Röhl, 2013). However, interpretation of the MECO at this site is complicated by the lack of a clear return to higher $\delta^{18}O$ values following the event and a hiatus which truncates the upper portion of the record (Edgar et al., 2010; Shipboard Scientific Party, 2004). IODP Site U1333 in the equatorial Pacific Ocean also has good age control with both a comprehensive magnetic stratigraphy and an orbitally tuned age model across the whole of the MECO interval (Expedition 320/321 Scientists, 2009; Westerhold et al., 2014), but its relatively deep paleo-water depth (~3.5 km), coupled with a relatively shallow Pacific CCD in the middle Eocene, resulted in little or no carbonate preservation across the peak of the event, preventing detection of its true magnitude (Expedition 320/321 Scientists, 2009; Pälike et al., 2012; Westerhold et al., 2014). Furthermore, no planktic foraminifera are present across the entire MECO interval at Site U1333 to constrain surface-water conditions. Similarly, at shallower ODP Site 1209 (~2 km paleo-water depth) in the subtropical North Pacific Ocean (Dutton et al., 2005) the interval containing the MECO has poor carbonate microfossil preservation, very low sedimentation rates and thus, poor age control (Dawber and Tripati, 2011; Shipboard Scientific Party, 2002).

Equatorial Pacific ODP Site 865 is an older site that has been rather neglected in Eocene paleoceanographic studies. Drilled on Allison Guyot in 1992 on ODP Leg 143, the recovered cores sample the pelagic sediment drape (~200 m thick at the centre, ~140 m

109 at Site 865 which was drilled off-centre) that accumulated during much of the Paleogene
110 and early Neogene. Existing studies reveal the sediments to comprise a succession of
111 Paleocene to Miocene foraminiferal-nannofossil ooze and foraminiferal sands
112 (Shipboard Scientific Party, 1993a). The relatively shallow paleo-water depths (<2 km)
113 on the guyot top maximizes the preservation potential of carbonate microfossils, thus
114 avoiding problems of CCD and lysocline shoaling encountered elsewhere at deeper sites
115 (e.g., IODP Site U1333). Several Paleogene-focused studies have highlighted the
116 potential of this site for paleoceanographic and evolutionary studies (Arreguín-
117 Rodríguez et al., 2016b; Bralower et al., 1995; Coxall et al., 2000; Edgar et al., 2015;
118 Norris and Nishi, 2001; Pearson and Ezard, 2014; Pearson and Palmer, 2000; Tripati et
119 al., 2003), but most of the high-temporal resolution work has focused on the Paleocene-
120 Eocene Thermal Maximum (PETM) (Kelly et al., 1996; Kozdon et al., 2011; Kozdon et al.,
121 2013; Tripati and Elderfield, 2004) since ODP Site 865 is one of the few open ocean sites
122 with carbonate present throughout the event.
123
124 Middle Eocene sediments at Site 865 have not received much attention for
125 paleoceanographic studies, in large part because of: (1) poor quality of shipboard
126 physical property records preventing the development of a composite section necessary
127 to develop continuous stratigraphic sections, (2) the lack of magnetic reversal or
128 cyclostratigraphy for age control, and (3) evidence for reworking of calcareous
129 microfossils, e.g., across the PETM onset and in the upper portions of the sediment
130 column (Bralower and Mutterlose, 1995; Kelly et al., 1998; Shipboard Scientific Party,
131 1993a). Reworking and winnowing of sediment is an acknowledged problem of guyot-
132 top sites where ocean currents can be locally intensified by the topography (Pearson,
133 1995). However, evolutionary work, has demonstrated that the calcareous microfossils,
134 are diverse and abundant, albeit recrystallized (Edgar et al., 2015; Pearson et al., 2001;
135 Sexton et al., 2006) providing an apparently complete sequence of tropical Paleogene

biomarkers and their lineage evolution (Coxall et al., 2000; Norris and Nishi, 2001; Pearson and Ezard, 2014). Importantly, existing biostratigraphic assessments for Holes 865B and 865C identify planktonic foraminiferal Zone E12, defined by the total range of *Orbulinoides beckmanni* and spanning the MECO interval, and calcareous nannofossil Zone CN15/NP16, although there are large (~1 m) recovery gaps between cores (Bralower and Mutterlose, 1995; Shipboard Scientific Party, 1993a). Core photos indicate the presence of carbonate-rich sediments throughout the entire interval of interest (i.e., there is no evidence of a clay horizon) providing a promising target for geochemical and plankton assemblage work worth further investment (Edgar et al., 2015; Pearson and Palmer, 2000; Shipboard Scientific Party, 1993a).

Here we take the first step towards developing the ODP Site 865 MECO sequence as a palaeoceanographic reference by adding new data sets that allow development of a refined and detailed chronostratigraphy for the site. This involves high-resolution X-ray fluorescence (XRF) core scanning, benthic foraminiferal stable isotope ($\delta^{13}C$ and $\delta^{18}O$), and planktic foraminiferal and calcareous nannofossil biostratigraphic data across the MECO interval at the site. These data are combined with published calcareous nannofossil datums (Bralower and Mutterlose, 1995) to: [1] generate the first composite sedimentary section across the middle Eocene interval of Site 865, [2] identify and constrain the isotopic character of the MECO in the Pacific Ocean, and [3] determine the position of key biostratigraphic datums relative to the MECO event.

## 2. Materials and Methods

### 2.1 Regional Setting

ODP Site 865 was recovered during ODP Leg 143 and is located on Allison Guyot in the western North Pacific Ocean at 18° 26.410'N, 179° 33.339'W and a modern water depth of 1516 m (Shipboard Scientific Party (1993a); Fig. 1). This guyot is just one of a number

of similar flat topped volcanic seamounts in the region formed during the Cretaceous (e.g., Resolution and Wodejebato Guyots), rising up several km from the surrounding abyssal (>4 km) seafloor (Matthews et al., 1974; Shipboard Scientific Party, 1993b). Three holes were drilled at Site 865 (A–C) with middle Eocene sediments only recovered in Holes B and C, which were cored to try and create a continuous record of this interval. The middle Eocene sequence at Site 865 is positioned at shallow burial depths (<100 m) with no significant Quaternary cover. The foraminiferal nannofossil ooze and foraminiferal sands are reconstructed to have been deposited at ~1300–1500 m paleo-water depth based on benthic foraminiferal assemblages (Shipboard Scientific Party, 1993a) in a fully pelagic ocean gyre setting characterized by year round thermal stratification (Pearson et al., 2001).

**2.2 X-Ray Fluorescence (XRF) Scanning**

XRF data are routinely employed for stratigraphic correlation and the construction of high-resolution composite depth scales because of their higher signal-to-noise ratio and more consistent hole-to-hole character than shipboard physical property measurements (Röhl and Abrams, 2000). Prior to XRF analysis, the top ~0.5 cm of the split section surface of the archive halves was scraped off with a glass slide. This revealed bioturbation structures, indicating that this interval did not have significant coring disturbance (as might be expected from the foraminifera-ooze lithologies and the massive appearance of the unprepared cores). Using an Avaatech XRF scanner with a Canberra X-PIPS SDD, Model SXD-150-500 X-ray detector, a suite of element (including Fe, Ca, Sr, and Ba) intensity data were collected every 2 cm down-core with a constant spot size (cross core slot = 12 mm, down-core slit = 10 mm) using a 6 or 10 second count time at 30 and 50 kV, respectively, on the split surface of the archive half of each section using the TAMU ODASES XRF scanner at the International Ocean Discovery Program (IODP) Gulf Coast Core Repository. We measured the elemental composition of

sediments that encompassed planktic foraminiferal Zone E12 from ODP Cores 865B-4H and 5H (27.52–44.58 mbsf) and Sections 865C-4H-1 to 6H-2 (22.34–42.80 mbsf) in order to capture overlapping sections and construct a composite splice. All XRF elemental data are reported in Supplementary Table 1.

### 2.3 Cyclostratigraphy

To investigate if orbital forcing drove patterns in the elemental data records, the Fe intensity data and the natural logarithm of Sr/Ca, ln(Sr/Ca), as measured at 30 kV, was subjected to time series analyses. The Fe intensity data were selected to allow comparison with published datasets (Westerhold and Röhl, 2013), and the ln(Sr/Ca) record for its low signal to noise ratio (see Section 3.1). Records were evenly sampled and periodicities larger than 7 m were removed in the program *AnalySeries* (Paillard et al., 1996). Spectral analyses were performed with *Redfit 3.8* (Schulz and Mudelsee, 2002) using a Welch window. The behavior of periodicities over the length of the dataset was investigated by evolutive harmonic analysis with the astrochron package in R (Meyers, 2014), using a window length of 5.5 m for ln(Sr/Ca) and 6 m for Fe intensity. The Fe record displays a stronger imprint of short-term (<1 m) variability than the ln(Sr/Ca) record. To test whether the observed cycle hierarchy in the Fe record can be confidently linked to an orbital origin, the interval with most persistent periodicities as identified in the evolutive spectrum, between 32.5 and 44.5 amcd, was investigated with the average spectral misfit (ASM) method in *astrochron* (Meyers, 2014). Bandpass filters were applied to the datasets centered at periodicities of 1.9 m and 50 cm with broad bandwidths of 1/3 of the center frequency. The ln(Sr/Ca) record displays a stronger imprint of longer (>1 m) periodicities than the Fe record, with minima in the 1.9-m bandpass filter of ln(Sr/Ca) generally coinciding with maxima in the 1.9-m bandpass filter of Fe. High Fe intensities generally coincide with intervals of higher variability in the Fe record, which are likely controlled by a larger amplitude of variation in the

orbital forcing parameters, during eccentricity maxima. In concordance with the approach of (Westerhold and Röhl, 2013), we consider eccentricity maxima to coincide with maxima in the Fe record, and therefore minima in the ln(Sr/Ca) record. A tentative orbital tuning was established by (i) anchoring the maximum in the 1.9-m bandpass filter of ln(Sr/Ca) to the 405 kyr eccentricity minimum at 40.5 Ma in the La2011 eccentricity solution (Laskar et al., 2011), and (ii) connecting consecutive maxima in the 1.9-m bandpass filter of ln(Sr/Ca) to 405 kyr eccentricity minima.

### 2.4 Planktic foraminiferal and calcareous nannofossil biostratigraphy

Biostratigraphic analysis was conducted on samples spanning the inferred MECO interval to identify both primary bioevents defining planktic foraminiferal zones and key secondary datums as defined by Berggren and Pearson (2005) and Wade et al. (2011). Biostratigraphic samples were taken between Sections 865B-4H-3 and -5H-2, (~30.60–39.98 meters below sea floor, mbsf) in Hole 865B and between Sections 865C-4H-1 and -6H-2 (~22.35–44.05 mbsf) in Hole 865C, initially at relatively low resolution but increasing to ~10–20 cm spacing close to key datums. The position of planktic foraminifer datums outside of the studied sample set were determined using shipboard biostratigraphic residues with one sample per core section (every ~1.5 m) and are as presented in Figure 1 of Pearson and Ezard (2014) from Coxall (*unpub.*). Taxonomy follows Pearson et al. (2006). We also present calcareous nannofossil datums determined by Bralower and Mutterlose (1995) and new nannofossil data based on analysis of an additional 20 samples from Sections 865B-4H-3 to -5H-1 and Sections 865C-4H-5 to -5H-5. We use Top (T) and Base (B) to describe the highest and lowest occurrences of taxa, and Top and Base common (Tc and Bc) for the highest and lowest common occurrences, respectively. Representative specimens of key biostratigraphically important taxa were selected for Scanning Electron Microscope

(SEM) analysis. Specimens were gold coated prior to analysis and SEM imaging was conducted on a Philips XL-30 Environmental SEM at the University of Birmingham.

### 2.5 Stable carbon and oxygen isotope measurements

Benthic foraminiferal stable isotope ($\delta^{13}C$ and $\delta^{18}O$) data were generated from the epifaunal taxon *Nuttallides truempyi* following the taxonomic concept of Holbourn et al. (2013). Foraminifers were picked from the 250–300 μm sieve size fraction and cleaned by ultrasonication to remove any loose fine material prior to stable isotope analysis. All stable isotope measurements were determined using a Thermo Scientific Delta V Advantage mass spectrometer coupled to a Gas Bench II in the School of Earth and Ocean Sciences at Cardiff University and are reported relative to the Vienna Pee Dee Belemnite (VPDB) standard. External analytical precision for $\delta^{13}C$ and $\delta^{18}O$ analyses is 0.06 and 0.07‰, respectively. No species-specific corrections are applied. Stable isotope data for Holes 865B and 865C are reported in Supplementary Tables 2 and 3, respectively.

## 3. Results

### *3.1. XRF data*

Despite initial concerns about coring disturbance and the lack of clear signals in the shipboard physical property datasets (Shipboard Scientific Party, 1993a), pronounced cyclicity is evident in the high-resolution XRF records throughout the study interval aiding correlation between holes (Fig. 2; Supplementary Table 1). Sr/Ca and Ba/Ca data are the most useful parameters for correlation because of the higher signal-to-noise ratio compared to other elemental ratios, e.g., Fe/Sr. These datasets enabled the construction of an unambiguous composite depth scale spanning a ~25-m interval between ~22 and 47 mbsf for the first time at Site 865 (Tables 1 and 2). This is the first core splice (and thus, official meters composite depth (mcd) scale) available for any

interval at Site 865. The biggest difference between the new mcd scale and the shipboard mbsf depth scale is that the core recovery gap between Cores 865C-4H and -5H has increased from ~1 to >3 m indicating that significant offsets must be applied. In order to maximize the sample material available for study, out-of-splice intervals were also correlated to the in-splice intervals through development of an 'adjusted' meters composite depth (amcd) scale (Tables 3 and 4; Fig. 2). This new amcd scale only applies to the intervals for which XRF are collected and thus, some of the bioevents reported in this study fall outside of this. This was achieved by aligning clearly identifiable common features in each hole, and defining mapping pairs (Tables 3 and 4) by stretching/squeezing of the out-of-splice core segments to match the in-splice intervals (Fig. 2). All interpretations below are considered relative to the final composite amcd scale. Note that it was not possible to align all features in the elemental records because of distortion (contraction and expansion) within each core. Also, since the intent of this work is to generate a composite section across the MECO interval, we do not focus here on the possible environmental implications of the XRF records.

**3.2 Cyclostratigraphy**

Spectral analysis of the ln(Sr/Ca) record by Redfit displays the most prominent periodicities at 1.9 m and 73 cm, and additional periodicities at 3.0 m, 2.4 m, 78 cm and 40 cm above the 95% confidence level, and at 60 cm above the 90% confidence level (Fig. 3). In the Fe record, periodicities above the 95% confidence level are detected at 6.3 m, 1.9–1.2 m and 63 cm (Fig. 3), with an additional periodicity of 49 cm above the 80% confidence level. Evolutive analyses track the behavior of the ~1.9 m and 40–78 cm periodicities over the length of the record, revealing reduced power at depths around 32.5 and 39.5 amcd. ASM analysis of the Fe intensity record from 32.5 to 44.5 m reveals a hierarchy of periodicities likely corresponding to an orbital imprint at a sedimentation rate of 0.46 cm/kyr (Supplementary Fig. 1). This is in close agreement with the average

297 sedimentation rate obtained from tuning to the 405-kyr eccentricity cycle at 0.48
298 cm/kyr on average over the entire record. A sedimentation rate of 0.48 cm/kyr would
299 translate the periodicity of 1.9 m, which is strongly present in the ln(Sr/Ca) record, to a
300 duration of 406 kyr, which is close to the periodicity of long eccentricity at 405 kyr.
301
302 ***3.2 Planktic foraminiferal biostratigraphy***
303 All of the samples analysed contain abundant recrystallised or 'frosty' planktic
304 foraminifera (See Fig. 6 and Edgar et al. (2015) for images of wall cross sections). The
305 assemblages are diverse and typical of tropical middle Eocene low latitude
306 environments. The dominant genera are *Acarinina, Morozovelloides*, *Turborotalia,*
307 *Globigerinatheka* and *Subbotina,* with minor but conspicuous contributions from
308 *Hantkenina, Guembelitrioides, Globanomalina,* and *Pseudohastigerina*. Thus, the
309 (sub)tropical planktic foraminifera zonation scheme of Berggren and Pearson (2005)
310 can easily be applied at this site and, unusually, a complete sequence of Eocene
311 biomarkers and biozones can be identified. From the pattern of evolutionary bioevents
312 recognized we identify planktic foraminiferal Zones E10–E15 within the study interval
313 (Table 5; Fig. 5). Images of planktic foraminiferal species of biostratigraphic significance
314 are shown in Figure 4.
315
316 The planktic foraminiferal biostratigraphic data serve two purposes: (i) comparison of
317 bioevents in Holes 865B and 865C to provide a check on XRF-based hole-to-hole
318 correlations, and (ii) critical age control for this site. The relative sequence and depths of
319 planktic foraminiferal datums in Holes 865B and 865C are in relatively good agreement
320 with one another on the new amcd scale, indicating no major misalignments based on
321 the XRF correlations. The top of *G. semiinvoluta,* defining the base of Zone E15, falls in
322 samples outside of the new splice (Table 5), occurring at 20.35±0.10 mbsf in Hole 865B
323 and at 21.57±0.79 mbsf in Hole 865C (and above 22.37 amcd). Small offsets between the

two holes support the minimal composite depth offsets in the uppermost cores (<0.78 m; Tables 1, 2 and 5; Figure S2). Unfortunately reworking of older into younger material is evident in the topmost samples investigated here (<31 amcd; Fig. 3) specifically early middle Eocene material is reworked into middle and late Eocene sediments. The most noticeable example of this is in the overlapping occurrences of *Globigerinatheka semiinvoluta* with the large A*carinina (e.g., A. praetopilensis* and *A. mcgowrani)* and *Morozovelloides (M. crassatus* and *M. lehneri),* and even *Morozovella aragonenesis* (from Zones E5-9) in Sections 865C-4H-1 to -4H-4. Reworking is not immediately evident in the topmost samples of the high-resolution sample set from Hole 865B. Fortunately reworked specimens are relatively easy to discern as they typically have a distinctive brown/orange stain, may contain small flecks of pyrite and are more poorly preserved, e.g., fragmented. We find no obvious evidence of down-hole contamination.

The evident reworking has several consequences for the biostratigraphic zonation. First, the Top of *M. crassatus* used to define the base of Zone E14 was not confidently identified here because significant numbers of individuals are present in both Cores 865B-3H and 865C-3H. Thus, the base of *G. semiinvoluta,* which is calibrated to the same age as the Top of *M. crassatus* was used to approximate the base of Zone E14 instead (27.61±1.01 mbsf in Hole 865B and 26.34±0.07 amcd in Hole 865C). The slight difference between the two horizons may reflect its relative rarity of this taxon and difficulties distinguishing *G. semiinvoluta* from its immediate ancestor *G. mexicana* at the base of its range (Premoli Silva et al., 2006) or that Cores 865B-3H and 865C-3H fall outside of the new amcd scale. In contrast, the Top of *O. beckmanni* is an easily identifiable datum that defines the base of Zone E13 and is well constrained in Hole 865B (32.14±0.06 amcd). This datum, however, falls in the core gap between Cores 865C-4H and -5H (33.00±2.10 amcd), and hence there is a large depth uncertainty on this datum in Fig. 5. The Base of *O. beckmanni,* and thus Zone E12, can be more difficult

to define because there is a continuous chronocline from its ancestor *G. euganea* and there is no simple taxonomic discrimination, especially as the holotype is a relatively un-extreme form (Edgar et al., 2010; Premoli Silva et al., 2006) but here we find highly developed spherical forms in the lowermost part of the species range at 40.89±0.07 amcd and 41.03±0.05 amcd in Holes 865B and 865C, respectively. The Top of *A. bullbrooki* occurs ~4 m above the first occurrence of *O. beckmanni* at both sites (36.30±0.06 in Hole 865B and 37.13±0.05 amcd in Hole 865C) with highly quadrate 'classic' *A. bullbrooki* forms (Berggren et al., 2006) present that are not obviously reworked. This provides a further informal correlative horizon and a check on the correlation between Holes 865B and 865C. Whilst not official biozone markers for this interval of the Eocene, the *Hantkenina* assemblage at this site is very well developed and these taxa may be useful accessory markers (Coxall and Pearson 2006). For instance, we note that *Hantkenina australis* appears in samples at ~43 amcd coincident with a pronounced isotopic excursion (Fig. 5, possible C19r event).

The lower portion of the study interval is assigned to Zones E10 and E11. The top of *Guembelitrioides nuttalli,* which defines the base of Zone E11, occurs at 46.62±0.1 amcd in Hole 865C but was not defined in Hole 865B (as it fell outside of the available sample set). Notably, a small number of individuals that share the morphology of *G. nuttalli* with the distinctive high spire, globular chambers and a pronounced rim (Olsson et al., 2006) but which lack supplementary apertures on the spiral side are present sporadically much higher in the site up to ~22 amcd (Fig. 4e-f). The extinction of the distinctive taxon *Morozovella aragonensis* defining the base of Zone E10 falls outside of the new splice at 48.01±0.76 and 47.99±3.94 mbsf in Holes 865B and 865C, respectively. In Hole 865C, this corresponds to the extinction occurring below 47.51 amcd. The base of the secondary marker species *G. index* occurs at 62.10±0.50 mbsf in Hole 865B, and the bases of *G. index* and *M. lehneri* occur at 56.96±0.56 mbsf in Hole 865C. These datums

typically occur in Zone E10 but occur well below the Top of *M. aragonensis* here (Table 5).

### *3.3. Calcareous nannofossil biostratigraphy*

Calcareous nannofossils at Site 865 are moderately well preserved, showing signs of etching and/or recrystallization but most specimens are identifiable to species level throughout. Biostratigraphically important calcareous nannofossil occurrences from Bralower and Mutterlose (1995) that fall within our study interval are collated here and where possible translated onto the new amcd scale (Table 6). Marker species in Holes 865B and 865C on the new amcd scale are in broad agreement with one another, i.e., datums in both holes overlap in depth space (Fig. 6). Datums that don't quite overlap in terms of depth space are: *N. fulgens*, *R. (D.) bisectus* (>10 μm), *C. solitus,* and *S. furcatolithoides*. This is likely a function of the relative rarity of these taxa within the cores making it difficult to discern the highest or lowest true occurrence and/or that they are frequently overgrown making identification difficult (Bralower and Mutterlose, 1995). However, it is clear from the datums that fall outside of the interval incorporated in the new amcd scale in one or both Holes 865B and 865C (e.g., Bases of *Chiasmolithus oamaruensis* and *Reticulofenestra umbilicus* and Top of *C. gigas and C. grandis*) that bioevents in Cores 865B-3H and 865C-3H occur at similar levels indicating limited offsets between Holes 865B and 865C. More significant offsets of up to 5 m are present between Holes 865B and 865C from Cores 865B-7H and 865C-7H downwards indicating that significant adjustments are needed to align the two holes (Table 6).

Consistent with Bralower and Mutterlose (1995), calcareous nannofossil Zones NP15–18 (Martini, 1971)can be clearly identified at Site 865 (Table 6). On the more recent 'CNE' zonation scheme (Agnini et al., 2014), the interval encompassing CNE Zones 12–17 is identified but zones CNE14–16 cannot be differentiated. This is because the 'CNE'

405 primary marker species are either: very rare at this site (*Cribrocentrum erbae*); occur in
406 the same narrow window at ~28.5 amcd (T *Sphenolithus obtusus* and Bc *Cribrocentrum*
407 *reticulatum,* defining the bases of Zones CNE16 and 14, respectively; Fig. 6); or between
408 ~28-32 amcd appear out of sequence, e.g., the Bc *C. reticulatum* is very shallow
409 compared, as are the T *S. furcatolithoides* and T *C. solitus,* which also show the largest
410 offsets between the two holes.
411
412 ***3.4 Benthic foraminiferal stable isotope results***
413 Benthic foraminiferal stable isotope records in both holes show similar patterns of
414 change and absolute stable isotope values throughout the record, and are well aligned
415 on the new amcd scale (Fig. 3). Benthic foraminiferal $\delta^{18}O$ values vary between 0.3 and
416 1.2‰ with a minimum $\delta^{18}O$ values initially recorded at ~43 amcd coincident with an
417 abrupt shift of 0.7‰ to more negative $\delta^{13}C$ values. $\delta^{18}O$ and $\delta^{13}C$ values subsequently
418 increase and then plateau between 42–37 amcd. At ~36.5 amcd, a second transient
419 negative $\delta^{13}C$ excursion of ~1‰ occurs, which is closely followed by a ~0.8‰ shift to
420 lower $\delta^{18}O$ values at 35 amcd. $\delta^{13}C$ values increase through this same interval and reach
421 maximum values at 34 amcd. $\delta^{18}O$ values then gradually increase and $\delta^{13}C$ gradually
422 decrease towards the top of the section at 24 amcd.
423
424 **4. Discussion**
425 ***4.1 Reworking***
426 Reworking of older foraminifera (from Zone P14 now E13/14) into younger material in
427 Cores 865B-1H to -3H was reported during shipboard analysis (Shipboard Scientific
428 Party, 1993a) coinciding with the occurrence of relatively 'soupy' sediments with a high
429 water content, a downcore transition to more cohesive sediments coincided with
430 reduced reworking. We demonstrate that reworking of planktic foraminifera extends
431 deeper than this transition but lessens considerably with increasing depth and is not

immediately evident below Sections 865B 4H-3 or 865C 4H-4 (Figs 3 and 4). Only discrete time intervals are obviously mixed into younger sediments, i.e., reworked material is sourced from sediments deposited during Zone E13 (as we find re-worked *Morozovelloides* and *Acarinina* but not *O. beckmanni* from Zone E12) along with much older sediments from Zones E6–9. Reworking is less evident within nannofossil assemblages, but rare occurrences of *C. gigas* and *N. fulgens* occur several meters above their highest consistent occurrences in Cores 865B-3H and -4H and 865C-3H and -4H. These occurrences are consistent with remobilization of similar aged sediments and deposition within the same interval (Bralower and Mutterlose, 1995). Down-hole contamination was not obvious within planktic foraminifera assemblages but was problematic within calcareous nannofossil samples and was attributed to contamination from the saw used to split the cores and the high water content of the cores (Bralower and Mutterlose, 1995).

Reworking is very common in the pelagic cap sequences atop guyots drilled during ODP Legs 143 and 144 in the equatorial Pacific, with the most intense reworking reported in the lowermost ~40 m of pelagic sediments deposited above the drowned carbonate platforms related to changes in local hydrography (Pearson, 1995; Premoli Silva et al., 1993). Less intense reworking is also observed at higher (i.e., younger) levels in pelagic cap sequences and is more limited to discrete horizons and time intervals (Pearson, 1995; Watkins et al., 1995). Reworked material is likely sourced from the edges of the guyot top and transported towards the centre by intensification of bottom-water currents deflected up over the guyot as well as other localized hydrographic features common to these settings, ultimately helping to generate the characteristic low dome-shaped sediment stack found on many Pacific guyots (Genin et al., 1989; Pearson, 1995).

458 ODP Site 865 sits in an oceanographically dynamic area, relatively close to the edge of
459 the guyot, where the sedimentary cap starts to thin, e.g., it lacks the thick Miocene-
460 Quaternary overburden of the guyot centre (Shipboard Scientific Party, 1993a). The
461 abraded appearance of reworked foraminifera (e.g., dull luster and fragmented)
462 suggests that they have been exposed to intense mechanical erosion, e.g., from currents
463 and/or a more intense transport history than the *in-situ* assemblage (Pilkey et al., 1969;
464 Maikelm, 1967). Whereas the pervasive brown foraminiferal discoloration on many
465 specimens, an oxidized iron stain, and pyrite likely reflect deposition in a low
466 sedimentation (and hence high current intensity) area with iron sourced from the
467 contemporaneous formation of manganese-phosphate hardgrounds or remobilized
468 from the lower limestone platform. Together these lines of evidence suggest a similar
469 reworking mechanism to that observed on other Pacific guyots (Pearson, 1995; Watkins
470 et al., 1995) with sediments mobilized from the low sedimentation margins of the guyot
471 top during discrete intervals of increased local current intensity, and temporarily mixed
472 into sediments closer to the center of the pelagic cap. Crucially currents around Site 865
473 were clearly sufficient to mix and remobilize sediments at times in the late middle
474 Eocene but not to scour the guyot top of sediments. Consistent with this hypothesis is a
475 reduction of sedimentation rates above ~32 amcd (Figs 5 and S2) coincident with the
476 zone of most intense reworking. Lower sedimentation rates, in addition to being
477 consistent with elevated current activity either removing sediment or preventing
478 deposition, would also reduce dilution of mixed components in sediments by *in-situ*
479 fauna making the reworking more evident. Regardless of reworking, the ability to
480 correlate the XRF records at the decimeter scale and the coherent stable isotope
481 stratigraphy throughout Cores 865B-4H to -6H and 865C-4H to -6H suggests that if
482 reworking is present it is relatively easy to avoid, not pervasive throughout the site, and
483 most critically has not obscured primary environmental signals.
484

### *4.2 Climatic events at ODP Site 865*

The long-term shift towards higher benthic foraminiferal $\delta^{18}O$ values observed through the Site 865 study interval (Fig. 5) is consistent with a previously published low-resolution benthic foraminiferal stable isotope record spanning the middle and upper Eocene at this site (Bralower et al., 1995; Coxall et al., 2000) as well as the global Eocene cooling trend (Bohaty and Zachos, 2003; Zachos et al., 2008). Superimposed on this long-term trend is a transient negative $\delta^{18}O$ excursion between ~35–36 amcd, within calcareous nannofossil and planktic foraminiferal Zones NP16 and E12, respectively, which is identified here as the MECO event (Fig. 5). The onset of the event is defined at the point where $\delta^{18}O$ begins to show a transition to lower values. The end of the event is less clearly defined, as at some other sites (Bohaty et al., 2009). However, the distinctive $\delta^{13}C$ maximum, which immediately follows the MECO (as in Bohaty et al., 2009) suggests that the abrupt increase in $\delta^{18}O$ values at 35 amcd likely marks the end of the event (see vertical yellow bar in Fig. 5). Indeed the gradual increase in $\delta^{18}O$ values that follows between ~30-35 amcd, is seen at ODP Sites 738 and 748 where the end of the event is clearly defined.

Our new XRF records allow us to create a composite record enabling us to capture the entire MECO event. However, very low sedimentation rates (<0.6 cm/kyr; Fig. 5 and Table S5) at this site compared to many other deep-sea sites (Bohaty and Zachos, 2003; Boscolo Galazzo et al., 2014; Edgar et al., 2010) mean that the event is highly condensed comprising a <1-m interval (Fig. 3). This is consistent with the reduced magnitude of the $\delta^{18}O$ excursion (~0.8‰ vs. 1.0-1.5‰) compared to elsewhere, the lack of a short (<50 kyr) negative $\delta^{13}C$ excursion coincident with peak MECO conditions (defined by the $\delta^{18}O$ minimum), and rapid apparent event onset (Boscolo Galazzo et al., 2014).

Because of its relatively shallow water sedimentation, Site 865 is a critical end-member for constraining the Pacific CCD response during the MECO and other Eocene shoaling events. Quantifying the amount, timing and pattern of CCD change across the MECO is essential to solving the so-called "carbon cycle conundrum" that the MECO currently poses (Sluijs et al., 2013). At >900 m, the CCD shoaling associated with the MECO is the largest known in the middle-to-late Eocene interval (shoaling from ~3.3-4.2 km paleowater depth; Pälike et al., 2012). Relatively continuous carbonate sedimentation across the event at ODP Site 865 suggests that the CCD did not shoal above ~1300–1500 m (the estimated paleowater depth of the site; Shipboard Scientific Party, 1993a) in the Pacific Ocean at this time providing a maximum limit of 3 km change.

The negative carbon and oxygen isotopic excursions represented here by only a single sample at ~ 43 amcd, in planktic foraminiferal Zone E11, immediately before a shift to more positive $\delta^{18}O$ values likely corresponds to the 'C19r event', a transient hyperthermal style event (<100 kyrs in duration) initially recognised at ODP Site 1260 in the equatorial Atlantic (Edgar et al., 2007). The C19r event is now also known from the South Atlantic at ODP Sites 1263 and 702 and referred to as the Late Lutetian Thermal Maximum (Westerhold et al., 2017). Similar to the MECO, the relatively small stable isotope excursions compared to elsewhere (0.4‰ and 0.2‰ vs. 1.5‰ and ~1.8‰, in $\delta^{13}C$ and $\delta^{18}O$ at ODP Sites 865 and 1260, respectively) are likely a function of the low sedimentation rates at this site (~0.4–0.6 cm/kyr vs. 2.0 cm/kyr at ODP Site 1260) compounded by lower sampling frequency and time averaging. This is the first record of the C19r event outside of the Atlantic Ocean and suggests that the C19r event is in fact global in nature and, as such, may be a valuable stratigraphic marker within the long >1 Myr planktic foraminiferal Zone E11 in which it falls.

A tentative astronomical tuning based on correlation of the band-pass filter of ln(Sr/Ca) to the 405-kyr component of eccentricity, anchoring the record near the onset of the MECO to the eccentricity minimum at 40.5 Ma (Westerhold and Röhl, 2013), is in close agreement with available biostratigraphic age control (Fig. 6). This interpretation places the peak $\delta^{18}O$ excursion during the MECO within a 405-kyr eccentricity maximum at 40.3 Ma, and the carbon-isotope maximum directly following the MECO coincides with the 405-kyr eccentricity minimum at 40.1 Ma, in agreement with Westerhold and Röhl (2013). The duration of the interval between the potential C19r event and the onset of the MECO is estimated at three and a half 405-kyr cycles or 1.4 Myr, which is longer than the duration estimated by Westerhold and Röhl (2013) at two and a half 405 kyr cycles, ~1 Myr. Unfortunately, a detailed comparison to existing cyclostratigraphic studies is hampered by uncertainty in the detection of the C19r event. The seemingly different duration estimate is in line with existing discrepancies between astrochronologies, notably in the reported length of magnetochron C19r, with duration estimates varying between 0.9 Myr (Westerhold and Röhl, 2013; Westerhold et al., 2015; Westerhold et al., 2014) and 1.5 Myr (Boulila et al., 2018).

### *4.3 Integrated biostratigraphic schemes and relationship to the MECO*

Whilst both calcareous nannofossil and planktic foraminiferal zonation schemes can be applied to ODP Site 865 and are in generally good agreement, there is significant disagreement in the post-MECO interval between ~30 and 35 amcd (Fig. 6). Taken at face value, planktic foraminifera indicate constant sedimentation rates of ~0.5 cm/kyr throughout this interval whereas calcareous nannofossil datums suggest a 3.5 Myr hiatus between 38.6 and 42.1 Ma. However, XRF-derived elemental and stable isotope datasets and cyclostratigraphic analysis do not indicate any large shifts at this level that might indicate an abrupt shift in environmental conditions through time (Figs 2, 3 and

5). The presence of the MECO event itself, which falls within this potential gap, also implies that a hiatus is unlikely.

It is instead likely that low sedimentation rates and sampling frequency make it difficult to discern closely spaced calcareous nannofossil bioevents at Site 865, e.g., Tops of *C. solitus* and *S. furcatolithoides,* which are calibrated to a 130-kyr interval (40.40–40.53 Ma). However, these events also occur much higher in the section than expected relative to the MECO event at this site, and they also overlap with the much younger Top of *S. obtusus* and Base of *C. reticulatum* (Fig. 5). Explanations could include: these bioevents are diachronous and/or are not well calibrated or there is significant reworking of calcareous nannofossils. Indeed this interval does show evidence of reworking (Fig. 3), which could make the Tops of species appear higher in the section than expected and introduce a degree of subjectivity in determining what is *in situ* versus reworked, enhanced bioturbation and/or high core water content during this interval may have further affected the datum levels. However, a number of recent studies have questioned the accuracy of long-standing calcareous nannofossil age calibrations (e.g., Agnini et al., 2014; Tori and Monechi, 2013). For instance, many *Chiasmolithus* bioevents are no longer included in the newest calcareous nannofossil zonation scheme because typically low and sporadic abundances of these species at many sites introduces significant uncertainty to reported datum levels (Agnini et al., 2014; Larrasoaña et al., 2008; Villa et al., 2008). We also do see differences in the relative positions of the first occurrences of *D. bisectus* (<10μm) and *D. bisectus/scrippsae* (>10μm) in multiple studies, but this likely arises because of taxonomic ambiguity that has been associated with identifying these taxa (e.g., Backman, 1987; Larrasoaña et al., 2008; Mita, 2001; Tori and Monechi, 2013). The very high Base of *C. reticulatum* at the site is perhaps the most problematic, but reports of the position of this event from other sites are also variable, ranging from magnetochron C20r to C18n.2n (a ~5 Myr interval; Fornaciari et al., 2010; Rivero-

590 Cuesta et al., 2019). However, given the sporadic and rare presence of *C. reticulatum* in
591 our own observations here, the most likely explanation is ecological bias at Site 865.
592 Similarly, *N. fulgens* is typically rare with an infrequent distribution at Site 865 and
593 elsewhere, reducing its biostratigraphic utility (Bown, 2005; Shamrock, 2010).
594
595 The Base of *O. beckmanni* is diachronous, with the species first appearing in the tropics
596 prior to the MECO but subsequently expanding to higher latitudes across the onset of
597 the MECO and inferred surface water warming (Edgar et al., 2010; Jovane et al., 2010;
598 Luciani et al., 2010). At Site 865, the Base of *O. beckmanni* precedes the MECO event
599 consistent with this hypothesis (Fig. 3). The Top of *O. beckmanni* occurs after the MECO
600 event at Site 865, as at ODP Site 1051 and in the Alano section in the Atlantic and
601 Tethyan Oceans, respectively (Edgar et al., 2010; Luciani et al., 2010), suggesting that
602 cooling of surface waters following the MECO was not directly responsible for its
603 extinction. Regardless, planktic foraminiferal Zone E12 is a good marker for the MECO
604 interval in (sub)tropical sediments that lack a stable isotope stratigraphy. The first
605 occurrence of *D. scrippsae* (= *D. bisectus* <10 μm) at low- and mid-latitude sites is also
606 used to approximate the beginning of the MECO event based on close correlation at a
607 number of sites in the Atlantic Ocean (Bohaty et al., 2009). The Base of *D. bisectus* <10
608 μm does occur within the MECO event at ODP Site 865 (Fig. 5).
609
610 The robust and cosmopolitan planktic foraminifera *A. bullbrooki* is a valuable secondary
611 marker close to the base of Zone E12 at 40.04 Ma (Gradstein et al., 2012; Wade et al.,
612 2011) when *O. beckmanni* is absent either due to its relatively high susceptibility to
613 mechanical damage and dissolution or limited (sub)tropical distribution (Edgar et al.,
614 2010). However, here we find that the Top of *A. bullbrooki* and the Base of *O. beckmanni*
615 are not synchronous as implied by the current biozonation scheme (Wade et al., 2011).
616 Whilst there can be a degree of subjectivity in the definition of *O. beckmanni* between

617 workers at the start of its range (Premoli Silva et al., 2006) this is not the case at ODP
618 Site 865 where highly spherical and distinctive forms are present in the lowermost
619 samples (assuming that downhole contamination is not a major issue; Fig. 4). There are
620 relatively few sites where both taxa are reported but at ODP Sites 1051 and 1260, in the
621 (sub)tropical Atlantic Ocean, the Top of *A. bullbrooki* also occurs significantly higher
622 than the Base of *O. beckmanni* before (Site 1051) or even after the MECO event (Site
623 1260) (Edgar et al., 2010; Shipboard Scientific Party, 1998, 2004). In the Contessa
624 section, Italy the Top of *A. bullbrooki* occurs significantly below the Base of *O. beckmanni*
625 and the MECO (Jovane et al., 2010). Either way, the events are not contemporaneous
626 suggesting that a significant revision of this datum is required.
627
628 Whilst *Hantkenina* is present in low abundance throughout the mid-late Eocene of Site
629 865 (Coxall et al., 2000), the transient appearance of rare *Hantkenina australis*, a
630 distinctive middle Eocene form with recurved tubulospines, is present at Site 865 within
631 the inferred C19r 'hyperthermal' event. This is surprising because this taxon is found
632 globally, but, unlike most other *Hantkenina* spp.*,* is most abundant at higher latitudes
633 and, thus, in cooler waters (Coxall and Pearson, 2006). The appearance of *Hantkenina*
634 *australis* may prove to be a future useful marker for C19r, an otherwise 'datum poor'
635 interval. Notably, previous transient incursions of more tropical species of *Hantkenina*
636 to high northern latitudes (>50°N) in the middle Eocene at ODP Site 647 has previously
637 been used to infer surface ocean warming around the C19r interval (Shipboard Scientific
638 Party, 1987). However, stratigraphic revision of ODP Site 647 by Firth et al. (2012)
639 places the lower *Hantkenina* incursion at the base of calcareous nannofossil Zone NP16
640 and close to the Magnetochron 18r/19n boundary, which is significantly later than the
641 C19r event but before the MECO – and inconsistent with the hypothesis of expansion of
642 the *Hantkenina* range in response to warming surface waters. Thus, instead may reflect
643 changes in upwelling or increased primary production (Coxall et al., 2007).

644

645 The top of *G. nuttalli* was introduced as the marker for the base of planktic foraminiferal
646 Zone E11 in 2005, based on correlations at ODP Site 1050 and 1051 (R.D. Norris cited
647 inBerggren and Pearson, 2005) to break up the otherwise very long multi-million year
648 Zone P12 from the earlier zonation scheme (Berggren et al., 1995). However,
649 occurrences of *G. nuttalli* (albeit small individuals) have now been found as high as Zone
650 E14 (i.e., above the MECO) in the Alano section in northern Italy with the highest
651 consistent occurrence in Zone E13 (Agnini et al., 2011). The datum level reported in
652 Table 5 (XX amcd) is the highest consistent occurrence of this taxon at Site 865, but,
653 similar to Alano, we do find at least sporadic occurrences of small individuals up
654 through Zones E13 and E14 that are not obviously reworked.
655

656 A number of bioevents within Zone E10 at Site 865 are out of sequence with respect to
657 the primary datum – the Top of *M. aragonensis* (43.26 Ma) - occurring above the Bases
658 of younger taxa *G. index* and *M. lehneri* (at 42.64 and 43.15 Ma, respectively*)*. It is the
659 highest occurrences of taxa that are most likely to be impacted by reworking. Yet *M.*
660 *aragonensis* specimens do not show distinctive staining or worn appearance at this level
661 (as they do higher up in Hole 865C where they are clearly reworked), and, whilst
662 individuals could be remobilized locally, a higher Top of *M. aragonensis* compared to *G.*
663 *index* is also evident in the Contessa section, Italy (Jovane et al., 2010).
664

665 Clearly more work is needed to confidently understand the relative patterns of
666 calcareous nannofossil and planktic foraminiferal datums in the middle Eocene,
667 particularly from the Pacific Ocean since most (if not all) calibrations are currently
668 based on Atlantic or Tethyan sediment sequences and indeed few sites where both
669 groups are inter-calibrated (e.g., Agnini et al., 2014; Berggren and Pearson, 2005).
670 Whilst many key tropical middle Eocene bioevents are identified at Site 865, the lack of

magnetic or confident astrochronology hinders determination of the absolute age of the events reported here. However, in the future, the high-resolution stable isotope and XRF records should enable the development of a more robust orbitally tuned age model here or allow correlation to sites elsewhere that do possess an independent reliable stratigraphy.

## *5. Conclusions*

In this study, we have developed new biostratigraphic, stable isotope, and XRF records that span the MECO event at ODP Site 865 in the tropical Pacific Ocean. This site possesses a surprisingly pronounced signal in XRF-derived elemental counts and ratios permitting us to construct a reliable composite section for Holes 865B and 865C that spans the late middle Eocene time interval (~38–43 Ma). Cyclicity observed in XRF datasets is likely orbitally paced, and a tentative astronomical tuning of the study section indicates consistently low sedimentation rates of ~0.4-0.6 cm/kyr, in agreement bio- and chemostratigraphic age calibrations and correlations to other sites. Benthic foraminiferal stable isotope data indicate that the MECO and the C19r events are present at Site 865, albeit relatively condensed. Planktic foraminiferal biostratigraphic events from the classic zonation schemes are recognized here and are generally in good agreement with calibrated stratigraphies, with the exception of anomalously high occurrences of *G. nuttalli, A. bullbrooki* and *M. aragonensis*. When considered alongside available calcareous nannofossil datums, there is some disagreement in terms of both the relative ordering and position of calcareous microfossil events, particular with respect to the MECO event, which, in the absence of an independent age model, acts as a key stratigraphic marker. Thus, further calibrations of these bioevents are necessary, particularly from the Pacific Ocean, which is poorly represented in current calibration schemes. Microfossil reworking is also evident in the topmost ~30 m of Site 865, indicating a dynamic local hydrography capable of remobilizing and mixing sediments

during the middle Eocene. ODP Site 865 is the first tropical record where the apparent entirety of the MECO event is preserved in carbonate bearing sediments, and, despite the reworking at this site, the primary environmental signals are preserved. Thus, ODP Site 865 represents a valuable site for future investigations into environmental and biotic change in the tropics during the MECO.

***Acknowledgements***

This research used samples provided by the International Ocean Discovery Program (IODP). The authors would like to thank Sandra Nederbragt for technical assistance with $\delta^{18}O$ and $\delta^{13}C$ analyses and Cardiff University undergraduate students Bo Fan Peng, Jonathon Gamble and Holly Welsby for help picking benthic foraminifera. Financial support to KME was provided in the form of NERC grants (NE/H016457/1 and NE/P013112/1), and a Leverhulme Early Career Fellowship (ECF-2013-608).

**Figure 1 – Location map for ODP Site 865 (solid star) and other low latitude sites discussed in the main text (open stars) on a 40 Ma reconstruction.** Paleolatitudes for each site are calculated from van Hinsbergen et al. (2015).

**Figure 2 – Sr/Ca and Ba/Sr records from ODP Holes 865B and 865C on the new adjusted metres composite depth (amcd) scale.** The in-splice intervals are indicated by the horizontal bars at the bottom of the figure.

**Figure 3 – Time series analyses of the ln(Sr/Ca) and Fe intensity data and tentative orbital tuning**. From left to right: the La2011 eccentricity solution (dark blue) and its 405 kyr bandpass filter (light blue) and the ln(Sr/Ca) record and the Fe intensity record flanked by their 1.9 m (black) and 50 cm (grey) bandpass filters and evolutive power spectra, with e1, e2 and e3 indicating the potential imprint of the 405,

125 and 95 kyr components of eccentricity, respectively. The evolutive spectra are topped by redfit power spectra with dashed lines showing the 99, 95, 90 and 80% confidence levels and with main periodicities indicated. Horizontal yellow bands indicate the position of the MECO and the C19r event. Horizontal grey dashed lines indicate tentative tuning tie-points between the ln(Sr/Ca) bandpass filter and the astronomical solution.

**Figure 4** - Scanning electron and light microscope images of biostratigraphically important taxa at ODP Site 865. (a and b) Sample ODP Hole 865C-4H-2, 25-27 cm, *Morozovelloides lehneri* – reworked specimens with distinctive brown/orange discoloration*;* (c and d) Sample ODP Hole 865C-4H-2, 85-87 cm, *Globigerinatheka semiinvoluta*; (e) Sample ODP Hole 865C-5H-1, 5-7 cm, *Orbulinoides beckmanni*; (f) Sample ODP Hole 865C-5H-4, 85-87 cm, *Acarinina bullbrooki*; (g) Sample ODP Hole 865C-4H-3, 95-97 cm, a reworked *Morozovella aragonensis*; (h) Sample ODP Hole 865C-5H-2, 45-47 cm, *Globigerinatheka index*; (i) Sample ODP Hole 865C-5H-2, 45-47 cm, *Morozovelloides lehneri*. All scale bars are 100 μm.

**Figure 5 – Benthic foraminiferal stable isotope records and age control points in ODP Holes 865B and 865C.** (a and b) $\delta^{18}O$ and $\delta^{13}C$ values are from multi-specimen analyses of *Nuttallides truempyi* (no vital effect correction has been applied). Gaps in the records represent intervals where no data was generated. (c) Planktic foraminiferal datums are from this study (Table 5). (d) Nannofossil biostratigraphic markers are from Bralower and Mutterlose (1995) with new data here (Table 6). Depth uncertainty on datums are indicated by vertical lines (black lines = amcd scale; grey line = top or bottom depth falls outside of amcd scale and is shown on mbsf) and where not visible are smaller than the symbol. (e) Sedimentation rates on amcd scale based on orbital tuning tie-points (Supplementary Table 4) The vertical yellow bars define the positions

of the Middle Eocene climatic optimum (MECO) and the possible C19r event. T = top; B= base; Bc = base of common occurrence. Note that only datums that fall within the new amcd scale are shown here.

**Figure 6 – Age–depth plot for ODP Site 865.** Only datums falling within the new adjusted meters composite depth (amcd) scale are included here. To see all calcareous microfossil datums from the study interval see Supplementary Figure 2. Planktic foraminiferal datums are from this study and H. Coxall *unpub*. (presented in Pearson and Ezard (2014)) (Table 5). Calcareous nannofossil datums are from this study and Bralower and Mutterlose (1995) (Table 6). Depth uncertainty on datums are indicated by vertical lines (black lines = amcd scale; grey line = top or bottom depth falls outside of amcd scale and is shown on mbsf) and where not visible are smaller than the symbol. Black diamonds are the tuning tie-points to the orbital solution (Supplementary Table 4). Ages are shown on the Gradstein et al. (2012) timescale. amcd = adjusted metres composite depth. Abbreviations of datums are T or B for Top or Base followed by the first letter of the genus and species name.

**Table 1 –** Composite depth offsets within splice for ODP Site 865.

**Table 2** - Splice tie-points for ODP Site 865.

**Table 3 –** Mapping pairs for adjusting mcd to amcd for ODP Hole 865B.

**Table 4** – Mapping pairs for adjusting mcd to amcd for ODP Hole 865C.

**Table 5** – Planktic foraminiferal datums in ODP Holes 865B and C.

**Table 6 –** Calcareous nannofossil datums in ODP Holes 865B and C.

**Supplementary Figure 1. Sedimentation rate estimate using the ASM method, applied to the Fe intensity records from 32.5 to 44.5 m.** The lowermost panel shows

779 MTM analyses of the data with confidence levels indicated. Vertical dashed bars indicate
780 periodicities detected above the 90% confidence level, that are compared to the
781 periodicities of long eccentricity at 405 kyr (E1), short eccentricity at 125 kyr (E2) and
782 95 kyr (E3), obliquity at 39.2 kyr (O) and precession at 23.1 (P1) and 21.8 (P2) kyr . The
783 sedimentation rates at which the optimal fit is achieved are indicated in the topmost
784 panels. The middle panels show that the significance level threshold (dashed line) is
785 passed, so that the null hypothesis of no orbital forcing can be rejected.
786
787 **Supplementary Figure 2. Age depth plot for ODP Site 865 on metres below**
788 **seafloor (mbsf) depth scale to assess degree of offset between cores pre-**
789 **alignment (and new amcd scale).** Planktic foraminiferal datums are from this study
790 and H. Coxall *unpub*. (presented in Pearson and Ezard (2014)) (Table 5). Calcareous
791 nannofossil datums are from this study and Bralower and Mutterlose (1995) (Table 6).
792 Depth uncertainty on datums are indicated by vertical lines and where not visible are
793 smaller than the symbol. Ages are shown on the Gradstein et al. (2012) timescale. amcd
794 = adjusted metres composite depth.
795
796 **Supplementary Table 1: Raw elemental intensity counts for ODP Holes 865B and**
797 **865C – (Too big to upload need to put in doi)**
798 **Supplementary Table 2: Benthic foraminifer (*Nuttallides truempyi*) stable isotope**
799 **analyses for ODP Hole 865B**
800 **Supplementary Table 3: Benthic foraminifer (*Nuttallides truempyi*) stable isotope**
801 **analyses for ODP Hole 865C**
802 **Supplementary Table 4: Tuning tie-points on adjusted' metres composite depth**
803 **(amcd).**
804
805

## 6. References


Agnini, C., Fornaciari, E., Giusberti, L., Grandesso, P., Lanci, L., Luciani, V., Muttoni, G., Paelike, H., Rio, D., Spofforth, D.J.A., Stefani, C., 2011. Integrated biomagnetostratigraphy of the Alano section (NE Italy): A proposal for defining the middle-late Eocene boundary. Geological Society of America Bulletin 123, 841-U110.

Agnini, C., Fornaciari, E., Raffi, I., Catanzariti, R., Pälike, H., Backman, J., Rio, D., 2014. Biozonation and biochronology of Paleogene calcareous nannofossils from low and middle latitudes. Newsletters on Stratigraphy 47, 131-181.

Arreguín-Rodríguez, G.J., Alegret, L., Thomas, E., 2016a. Late Paleocene-middle Eocene benthic foraminifera on a Pacific seamount (Allison Guyot, ODP Site 865): Greenhouse climate and superimposed hyperthermal events. Paleoceanography 31, 346-364.

Arreguín-Rodríguez, G.J., Alegret, L., Thomas, E., 2016b. Late Paleocene-middle Eocene benthic foraminifera on a Pacific seamount (Allison Guyot, ODP Site 865): Greenhouse climate and superimposed hyperthermal events. Paleoceanography, n/a-n/a.

Backman, J., 1987. Quantitative calcareous nannofossil biochronology of middle Eocene through early Oligocene sediment from DSDP Sites 522 and 523. Abh. Geol. B.-A 39, 21-31.

Berggren, W.A., Kent, D.V., Swisher III, C.C., Aubry, M.-P., 1995. A revised Cenozoic geochronology and chronostratigraphy, Geochronology Time Scales and Global Stratigraphci Correlation Special Publication. Society for Sedimentary Geology (SEPM).

Berggren, W.A., Pearson, P.N., 2005. A Revised Tropical to Subtropical Paleogene Planktonic Foraminiferal Zonation. The Journal of Foraminiferal Research 35, 279-298.

Bijl, P.K., Houben, A.J.P., Schouten, S., Bohaty, S.M., Sluijs, A., Reichart, G.-J., Sinninghe Damsté, J.S., Brinkhuis, H., 2010. Transient Middle Eocene Atmospheric CO2 and Temperature Variations. Science 330, 819-821.

Bohaty, S.M., Zachos, J.C., 2003. Significant Southern Ocean warming event in the late middle Eocene. Geology 31, 1017-1020.

Bohaty, S.M., Zachos, J.C., Florindo, F., Delaney, M.L., 2009. Coupled greenhouse warming and deep-sea acidification in the middle Eocene. Paleoceanography 24, PA2207.

Boscolo Galazzo, F., Thomas, E., Giusberti, L., 2015. Benthic foraminiferal response to the Middle Eocene Climatic Optimum (MECO) in the South-Eastern Atlantic (ODP Site 1263). Palaeogeography, Palaeoclimatology, Palaeoecology, 432-444.

Boscolo Galazzo, F., Thomas, E., Pagani, M., Warren, C., Luciani, V., Giusberti, L., 2014. The middle Eocene climatic optimum (MECO): A multiproxy record of paleoceanographic changes in the southeast Atlantic (ODP Site 1263, Walvis Ridge). Paleoceanography, 2014PA002670.

Boulila, S., Vahlenkamp, M., De Vleeschouwer, D., Laskar, J., Yamamoto, Y., Pälike, H., Kirtland Turner, S., Sexton, P., Westerhold, T., Röhl, U., 2018. Towards a robust and consistent middle Eocene astronomical timescale. Earth and Planetary Science Letters 486, 94-107.

Bown, P., 2005. Palaeogene calcareous nannofossils from the Kilwa and Lindi areas of coastal Tanzania (Tanzania Drilling Project Sites 1 to 10, 2003-4). Journal of Nannoplankton Research 27, 21-95.
Bralower, T.J., Mutterlose, J., 1995. Calcareous nannofossil biostratigraphy of Site 865, Allison Guyot, central Pacific Ocean: A tropical Paleogene reference section, Proceedings of the Ocean Drilling Program, Scientific Results. Ocean Drilling Program, College Station Tex, pp. 31-74.
Bralower, T.J., Zachos, J.C., Thomas, E., Parrow, M., Paull, C.K., Kelly, D.C., Silva, I.P., Sliter, W.V., Lohmann, K.C., 1995. Late Paleocene to Eocene paleoceanography of the equatorial Pacific Ocean: Stable isotopes recorded at Ocean Drilling Program Site 865, Allison Guyot. Paleoceanography 10, 841-865.
Coxall, H.K., Pearson, P.N., 2006. Taxonomy, biostratigraphy, and phylogeny of the Hantkeninidae (Clavigerinella, Hantkenina, and Cribrohantkenina). Cushman Foundation for Foraminiferal Research Special Publication 41, 213-256.
Coxall, H.K., Pearson, P.N., Shackleton, N.J., Hall, M.A., 2000. Hantkeninid depth adaptation: An evolving life strategy in a changing ocean. Geology 28, 87-90.
Coxall, H.K., Wilson, P.A., Pearson, P.N., Sexton, P.F., 2007. Iterative evolution of digitate planktonic foraminifera. Paleobiology 33, 495-516.
Cramwinckel, M.J., van der Ploeg, R., Bijl, P.K., Peterse, F., Bohaty, S., Röhl, U., Schouten, S., Middleburg, J., Sluijs, A., 2019. Harmful algae and export production collapse in the equatorial Atlantic during the zenith of Middle Eocene Climatic Optimum warmth. Geology 47, 247-250.
Dawber, C.F., Tripati, A.K., 2011. Constraints on glaciation in the middle Eocene (46–37 Ma) from Ocean Drilling Program (ODP) Site 1209 in the tropical Pacific Ocean. Paleoceanography 26.
Dutton, A., Lohmann, K.C., Leckie, R.M., 2005. Insights from the Paleogene tropical Pacific: Foraminiferal stable isotope and elemental results from Site 1209, Shatsky Rise. Paleoceanography 20.
Edgar, K.M., Anagnostou, E., Pearson, P.N., Foster, G.L., 2015. Assessing the impact of diagenesis on $\delta$11B, $\delta$13C, $\delta$18O, Sr/Ca and B/Ca values in fossil planktic foraminiferal calcite. Geochimica et Cosmochimica Acta 166, 189-209.
Edgar, K.M., Bohaty, S.M., Gibbs, S.J., Sexton, P.F., Norris, R.D., Wilson, P.A., 2013. Symbiont 'bleaching' in planktic foraminifera during the Middle Eocene Climatic Optimum. Geology 41, 15-18.
Edgar, K.M., Wilson, P.A., Sexton, P.F., Gibbs, S.J., Roberts, A.P., Norris, R.D., 2010. New biostratigraphic, magnetostratigraphic and isotopic insights into the Middle Eocene Climatic Optimum in low latitudes. Palaeogeogr Palaeocl 297, 670-682.
Edgar, K.M., Wilson, P.A., Sexton, P.F., Suganuma, Y., 2007. No extreme bipolar glaciation during the main Eocene calcite compensation shift. Nature 448, 908-911.
Expedition 320/321 Scientists, 2009. Site U1333, in: Palike, H., Lyle, M., Nishi, H., Raffi, I., Gamage, K., Klaus, A. (Eds.), Proceedings of the Integrated Ocean Drilling Program. Integrated Ocean Drilling Program Management International, Inc., Texas A&M University.
Firth, J.V., Eldrett, J.S., Harding, I.C., Coxall, H.K., Wade, B.S., 2012. Integrated biomagnetochronology for the Palaeogene of ODP Hole 647A: implications for correlating palaeoceanographic events from high to low latitudes. Geological Society, London, Special Publications 373.

Fornaciari, E., Agnini, C., Catanzariti, R., Rio, D., Bolla, E.M., Valvasoni, E., 2010. Mid-latitude calcareous nannofossil biostratigraphy and biochronology across the middle to late Eocene transition. Stratigraphy 7, 229-264.
Genin, A., Noble, M., Lonsdale, P.F., 1989. Tidal currents and anticyclonic motions on two North Pacific seamounts. Deep Sea Research Part A. Oceanographic Research Papers 36, 1803-1815.
Gradstein, F.M., Ogg, J.G., Schmitz, M., Ogg, G., 2012. The Geologic Time Scale 2012 2-Volume Set. Elsevier, Boston, USA.
Holbourn, A., Henderson, A.S., MacLeod, N., 2013. Atlas of benthic foraminifera. John Wiley & Sons.
Jovane, L., Florindo, F., Coccioni, R., Dinarès-Turell, J., Marsili, A., Monechi, S., Roberts, A.P., Sprovieri, M., 2007. The middle Eocene climatic optimum event in the Contessa Highway section, Umbrian Apennines, Italy. Geological Society of America Bulletin 119, 413-427.
Jovane, L., Sprovieri, M., Coccioni, R., Florindo, F., Marsili, A., Laskar, J., 2010. Astronomical calibration of the middle Eocene contessa Highway section (Gubbio, Italy). Earth and Planetary Science Letters 298, 77-88.
Kelly, C.D., Bralower, T.J., Zachos, J.C., Silva, I.P., Thomas, E., 1996. Rapid diversification of planktonic foraminifera in the tropical Pacific (ODP Site 865) during the late Paleocene thermal maximum. Geology 24, 423-426.
Kelly, D.C., Bralower, T.J., Zachos, J.C., 1998. Evolutionary consequences of the latest Paleocene thermal maximum for tropical planktonic foraminifera. Palaeogeography, Palaeoclimatology, Palaeoecology 141, 139-161.
Kozdon, R., Kelly, D.C., Kita, N.T., Fournelle, J.H., Valley, J.W., 2011. Planktonic foraminiferal oxygen isotope analysis by ion microprobe technique suggests warm tropical sea surface temperatures during the Early Paleogene. Paleoceanography 26, PA3206.
Kozdon, R., Kelly, D.C., Kitajima, K., Strickland, A., Fournelle, J.H., Valley, J.W., 2013. In situ $\delta$ 18O and Mg/Ca analyses of diagenetic and planktic foraminiferal calcite preserved in a deep-sea record of the Paleocene-Eocene thermal maximum. Paleoceanography 28, 517-528.
Larrasoaña, J.C., Gonzalvo, C., Molina, E., Monechi, S., Ortiz, S., Tori, F., Tosquella, J., 2008. Integrated magnetobiochronology of the Early/Middle Eocene transition at Agost (Spain): Implications for defining the Ypresian/Lutetian boundary stratotype. Lethaia 41, 395-415.
Laskar, J., Gastineau, M., Delise, J.-B., Farrés, A., Fienga, A., 2011. Strong chaos induced by close encounters with Ceres and Vesta. Astronomy and Astrophysics 532.
Luciani, V., Giusberti, L., Agnini, C., Fornaciari, E., Rio, D., Spofforth, D.J.A., Pälike, H., 2010. Ecological and evolutionary response of Tethyan planktonic foraminifera to the middle Eocene climatic optimum (MECO) from the Alano section (NE Italy). Palaeogeography, Palaeoclimatology, Palaeoecology 292, 82-95.
Martini, E., 1971. Standard Tertiary calcareous nannoplankton zonation, in: Farninacci, A. (Ed.), Proceedings of the II Plankton Conference Roma. Tecnoscienza, Rome.
Matthews, J.L., Heezen, B.C., Catalano, R., Coogan, A., Tharp, M., Natland, J., Rawson, M., 1974. Cretaceous Drowning of Reefs on Mid-Pacific and Japanese Guyots. Science 184, 462-464.

Meyers, S.R., 2014. Astrochron: An R Package for Astrochronology. .
Mita, I., 2001. Data Report: Early to late Eocene calcareous nannofossil assemblages of Sites 1051 and 1052, Blake Nose, North western Atlantic Ocean, in: Kroon, D., Norris, R.D., Klaus, A. (Eds.), Proceedings of the Ocean Drilling Program, Scientific Reports. Ocean Drilling Program, College Station, TX, pp. 1-28.
Möbius, I., Friedrich, O., Edgar, K.M., Sexton, P.F., 2015. Episodes of intensified biological productivity in the subtropical Atlantic Ocean during hte termination of the Middle Eocene Climatic Optimum. Paleoceanography.
Norris, R., Nishi, H., 2001. Evolutionary trends in coiling of tropical Paleogene planktic foraminifera. Paleobiology 27, 327-347.
Olsson, R.K., Pearson, P.N., Huber, B.T., 2006. Taxonomy, biostratigraphy and phylogeny of Eocene Catapsydrax, Globorotaloides, Guembelitrioides, Paragloborotalia, Parasubbotina, and Pseudoglobigerinella n. gen., in: Pearson, P.N., Olsson, R.K., Huber, B.T., Hemleben, C., Berggren, W.A., Coxall, H.K. (Eds.), Atlas of Eocene Planktonic Foraminifera, 1 ed. Cushman Foundation, Fredericksburg, USA, pp. 67-110.
Paillard, D., Labeyrie, L., Yiou, P., 1996. Macintosh Program performs time-series analysis. Eos, Transactions American Geophysical Union 77, 379-379.
Pälike, H., Lyle, M.W., Nishi, H., Raffi, I., Ridgwell, A., Gamage, K., Klaus, A., Acton, G., Anderson, L., Backman, J., Baldauf, J., Beltran, C., Bohaty, S.M., Bown, P., Busch, W., Channell, J.E.T., Chun, C.O.J., Delaney, M., Dewangan, P., Jones, T.D., Edgar, K.M., Evans, H., Fitch, P., Foster, G.L., Gussone, N., Hasegawa, H., Hathorne, E.C., Hayashi, H., Herrle, J.O., Holbourn, A., Hovan, S., Hyeong, K., Iijima, K., Ito, T., Kamikuri, S., Kimoto, K., Kuroda, J., Leon-Rodriguez, L., Malinverno, A., Moore, T.C., Murphy, B.H., Murphy, D.P., Nakamura, H., Ogane, K., Ohneiser, C., Richter, C., Robinson, R., Rohling, E.J., Romero, O., Sawada, K., Scher, H., Schneider, L., Sluijs, A., Takata, H., Tian, J., Tsujimoto, A., Wade, B.S., Westerhold, T., Wilkens, R., Williams, T., Wilson, P.A., Yamamoto, Y., Yamamoto, S., Yamazaki, T., Zeebe, R.E., 2012. A Cenozoic record of the equatorial Pacific carbonate compensation depth. Nature 488, 609-+.
Pearson, P., 1995. Planktonic foraminifer biostratigraphy and the development of pelagic caps on guyots in the Marshall Islands group, Proceedings of the Ocean Drilling Program. Scientific results. Ocean Drilling Program, pp. 21-59.
Pearson, P.N., Ditchfield, P.W., Singano, J., Harcourt-Brown, K.G., Nicholas, C.J., Olsson, R.K., Shackleton, N.J., Hall, M.A., 2001. Warm tropical sea surface temperatures in the Late Cretaceous and Eocene epochs. Nature 413, 481-487.
Pearson, P.N., Ezard, T.H.G., 2014. Evolution and speciation in the Eocene planktonic foraminifer Turborotalia. Paleobiology 40, 130-143.
Pearson, P.N., Olsson, R.K., Huber, B.T., Hemleben, C., Berggren, W.A., Coxall, H.K., 2006. Atlas of Eocene Planktonic Foraminifera. Cushman Foundation, Fredericksburg, USA.
Pearson, P.N., Palmer, M.R., 2000. Atmospheric carbon dioxide concentrations over the past 60 million years. Nature 406, 695-699.
Premoli Silva, I., Haggerty, J., Rack, F., Party, S.S., 1993. Proceedings of the Ocean Drilling Program Initial Reports. Ocean Drilling Program, College Station, Texas.
Premoli Silva, I., Wade, B.S., Pearson, P.N., 2006. TAXONOMY, BIOSTRATIGRAPHY, AND PHYLOGENY OF GLOBIGERINATHEKA AND ORBULINOIDES, in: Pearson, P.N., Olsson, R.K., Huber, B.T., Hemleben, C.,

Berggren, W.A. (Eds.), Atlas of Eocene Planktonic Foraminifera, 1 ed. Cushman Foundation Special Publication, pp. 169-212.
Rivero-Cuesta, L., Westerhold, T., Agnini, C., Dallanave, E., Wilkens, R.H., Alegret, L., Paleoenvironmental Changes at ODP Site 702 (South Atlantic): Anatomy of the Middle Eocene Climatic Optimum. Paleoceanography and Paleoclimatology n/a.
Rivero-Cuesta, L., Westerhold, T., Agnini, C., Dallanave, E., Wilkens, R.H., Alegret, L., 2019. Paleoenvironmental Changes at ODP Site 702 (South Atlantic): Anatomy of the Middle Eocene Climatic Optimum. Paleoceanography and Paleoclimatology 34, 2047-2066.
Röhl, U., Abrams, L.J., 2000. High resolution, downhole, and nondestructive core measurements from sites 999 and 1001 in the Caribbean Sea: Application to the late Paleocene thermal maximum, in: Leckie, R.M., Sigurdsson, H., Acton, G.D., Draper, G. (Eds.), Proceedings of the Ocean Drilling Program, Scientific Results, College Station, TX, pp. 191-203.
Savian, J., Jovane, L., Trindade, R., Frontalini, F., Coccioni, R., Bohaty, S., Wilson, P., Florindo, F., Roberts, A., 2013. Middle Eocene Climatic Optimum (MECO) in the Monte Cagenero section, central Italy. Latinmag Letters 3.
Schulz, M., Mudelsee, M., 2002. REDFIT: estimating red-noise spectra directly from unevenly spaced paleoclimatic time series. Computers & Geosciences 28, 421-426.
Sexton, P.F., Norris, R.D., Wilson, P.A., Palike, H., Westerhold, T., Rohl, U., Bolton, C.T., Gibbs, S., 2011. Eocene global warming events driven by ventilation of oceanic dissolved organic carbon. Nature 471, 349-352.
Sexton, P.F., Wilson, P.A., Pearson, P.N., 2006. Microstructural and geochemical perspectives on planktic foraminiferal preservation: "Glassy'' versus "Frosty''. Geochemistry Geophysics Geosystems 7.
Shamrock, J.L., 2010. A new calcareous nannofossil species of the genus Sphenolithus from the Middle Eocene (Lutetian) and its biostratigraphic significance. Journal of Nannoplankton Research 31, 5-10.
Shipboard Scientific Party, 1987. Site 647, in: Srivastava, S.P., Arthur, M.A., Clement, B. (Eds.), Proceedings of the Ocean Drilling Program, Initial Reports. Ocean Drilling Program, Texas A&M University.
Shipboard Scientific Party, 1993a. Site 865, in: Sager, W.W., Winterer, E.L., Firth, J.V., Party, S.S. (Eds.), Proceedings of the Ocean Drilling Program, Initial Reports 143. Ocean Drilling Program, College Station, TX pp. 111-180.
Shipboard Scientific Party, 1993b. Synthesis of Results, Leg 143, in: Sager, W.W., Winterer, E.L., Firth, J.V., Party, S.S. (Eds.), Proceedings of the Ocean Drilling Program, Initial Reports 143. Ocean Drilling Program, College Station, TX
Shipboard Scientific Party, 1998. Site 1051, in: Norris, R.D., Kroon, D., Klaus, A., Party, S.S. (Eds.), Proceedings of the Ocean Drilling Program, Initial Reports. Ocean Drilling Program, College Station, TX.
Shipboard Scientific Party, 2002. Site 1209, in: Bralower, T.J., Premoli-Silva, I., Malone, M.J., Shipboard Scientific Party (Eds.), Proceedings Ocean Drilling Project Initial Reports. Ocean Drilling Program, College Station, TX, pp. 1-102.
Shipboard Scientific Party, 2004. Site 1260, in: Erbacher, J., Mosher, D.C., Malone, M.J., Party, S.S. (Eds.), Proceedings of the Ocean Driling Project Initial Reports. Ocean Drilling Program, College Station, TX, pp. 1-113.

1046 Spofforth, D.J.A., Agnini, C., Pälike, H., Rio, D., Fornaciari, E., Giusberti, L., Luciani,
1047 V., Lanci, L., Muttoni, G., 2010. Organic carbon burial following the middle Eocene
1048 climatic optimum in the central western Tethys. Paleoceanography 25, PA3210.
1049 Tori, F., Monechi, S., 2013. Lutetian calcareous nannofossil events in the Agost
1050 section (Spain): implications toward a revision of the Middle Eocene
1051 biomagnetostratigraphy. Lethaia 46, 293-307.
1052 Tripati, A.K., Delaney, M.L., Zachos, J.C., Anderson, L.D., Kelly, D.C., Elderfield, H.,
1053 2003. Tropical sea‐surface temperature reconstruction for the early Paleogene
1054 using Mg/Ca ratios of planktonic foraminifera. Paleoceanography 18.
1055 Tripati, A.K., Elderfield, H., 2004. Abrupt hydrographic changes in the equatorial
1056 Pacific and subtropical Atlantic from foraminiferal Mg/Ca indicate greenhouse
1057 origin for the thermal maximum at the Paleocene-Eocene Boundary.
1058 Geochemistry, Geophysics, Geosystems 5, Q02006.
1059 van Hinsbergen, D.J.J., de Groot, L.V., van Schaik, J., Spakman, W., Bijl, P.K., Sluijs,
1060 A., Langereis, C.G., Brinkhuis, H., 2015. A Paleolatitude Calculator for
1061 Paleoclimate Studies. PLoS ONE 10.
1062 Villa, G., Fioroni, C., Pea, L., Bohaty, S., Persico, D., 2008. Middle Eocene–late
1063 Oligocene climate variability: Calcareous nannofossil response at Kerguelen
1064 Plateau, Site 748. Mar Micropaleontol 69, 173-192.
1065 Wade, B.S., Pearson, P.N., Berggren, W.A., Pälike, H., 2011. Review and revision of
1066 Cenozoic tropical planktonic foraminiferal biostratigraphy and calibration to the
1067 geomagnetic polarity and astronomical time scale. Earth-Science Reviews 104,
1068 111-142.
1069 Watkins, D.K., Pearson, P.N., Erba, E., Rack, F., Premoli Silva, I., Bohrmann, H.W.,
1070 Fenner, J., Hobbs, P.N., 1995. Stratigraphy and Sediment Accumulation Patterns
1071 of the Upper Cenozoic Pelagic Carbonate Caps of Guyots in the Northwestern
1072 Pacific Ocean, in: Haggerty, J., Premoli Silva, I., Rack, F., McNutt, M.K. (Eds.),
1073 Proceedings of the Ocean Drilling Program Scientific Reports. Ocean Drilling
1074 Program, College Station, TX.
1075 Westerhold, T., Röhl, U., 2013. Orbital pacing of Eocene climate during the Middle
1076 Eocene Climate Optimum and the chron C19r event: Missing link found in the
1077 tropical western Atlantic. Geochemistry, Geophysics, Geosystems 14, 4811-4825.
1078 Westerhold, T., Röhl, U., Donner, B., Frederichs, T., Kordesch, W.E.C., Bohaty, S.M.,
1079 Hodell, D.A., Laskar, J., Zeebe, R.E., Late Lutetian Thermal Maximum—Crossing a
1080 Thermal Threshold in Earth's Climate System? Geochemistry, Geophysics,
1081 Geosystems, n/a-n/a.
1082 Westerhold, T., Röhl, U., Donner, B., Frederichs, T., Kordesch, W.E.C., Bohaty, S.M.,
1083 Hodell, D.A., Laskar, J., Zeebe, R.E., 2017. Late Lutetian Thermal Maximum—
1084 Crossing a Thermal Threshold in Earth's Climate System? Geochemistry,
1085 Geophysics, Geosystems 19.
1086 Westerhold, T., Röhl, U., Frederichs, T., Bohaty, S.M., Zachos, J.C., 2015.
1087 Astronomical calibration of the geological timescale: closing the middle Eocene
1088 gap. Clim. Past 11, 1181-1195.
1089 Westerhold, T., Röhl, U., Pälike, H., Wilkens, R., Wilson, P.A., Acton, G., 2014.
1090 Orbitally tuned timescale and astronomical forcing in the middle Eocene to early
1091 Oligocene. Clim. Past 10, 955-973.
1092 Witkowski, J., Bohaty, S.M., Edgar, K.M., Harwood, D.M., 2014. Rapid fluctuations
1093 in mid-latitude siliceous plankton production during the Middle Eocene Climatic

Optimum (ODP Site 1051, western North Atlantic). Mar Micropaleontol 106, 110-129.
Zachos, J.C., Dickens, G.R., Zeebe, R.E., 2008. An early Cenozoic perspective on greenhouse warming and carbon-cycle dynamics. Nature 451, 279.

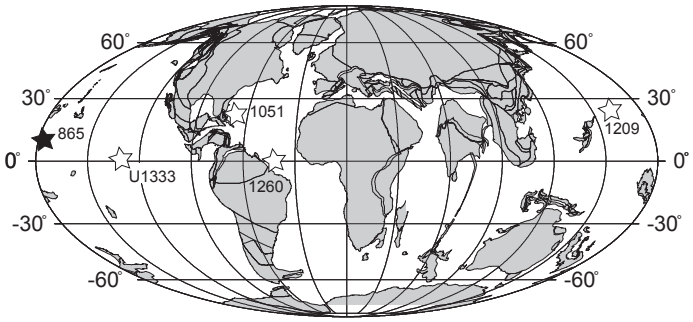
60°
60°
30°
30°
0°
0°
-30°
-30°
-60°
-60°
865
U1333
1051
1260
1209

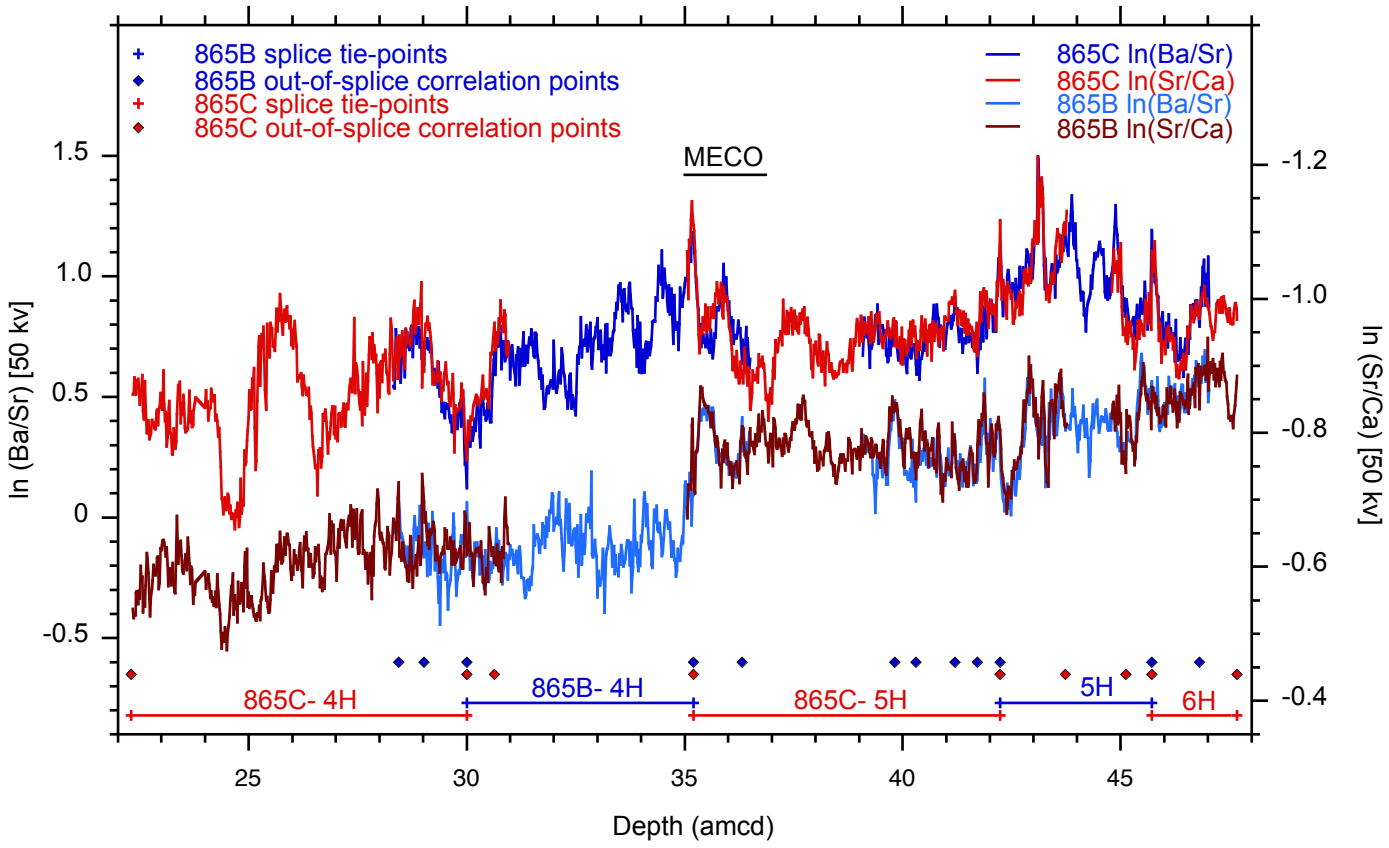
865B splice tie-points
865B out-of-splice correlation points
865C splice tie-points
865C out-of-splice correlation points
865C ln(Ba/Sr)
865C ln(Sr/Ca)
865B ln(Ba/Sr)
865B ln(Sr/Ca)
MECO
ln (Ba/Sr) [50 kv]
ln (Sr/Ca) [50 kv]
1.5
1.0
0.5
0
-0.5
-1.2
-1.0
-0.8
-0.6
-0.4
865C- 4H
865B- 4H
865C- 5H
5H
6H
25
30
35
40
45
Depth (amcd)

Edgar_Figure 3

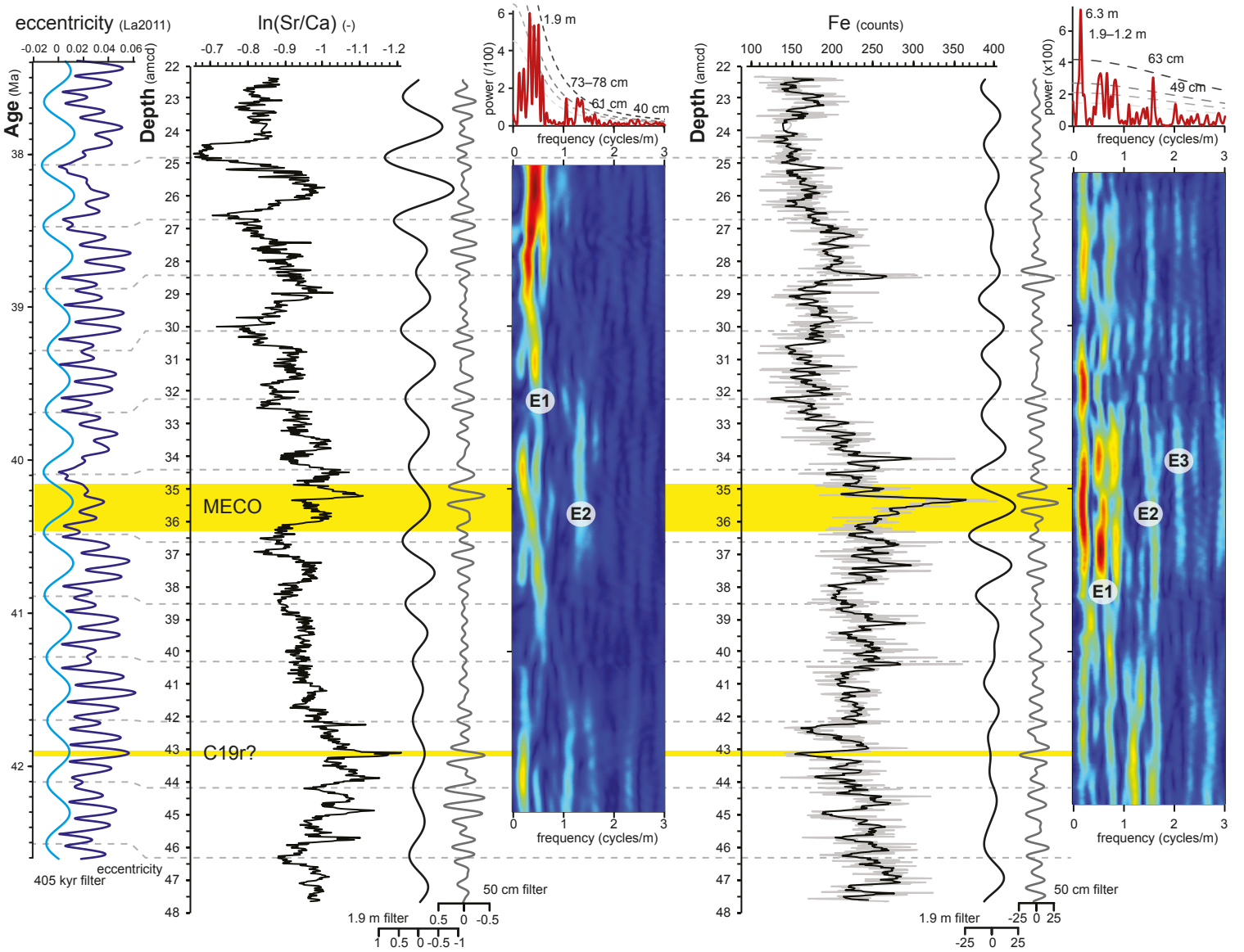

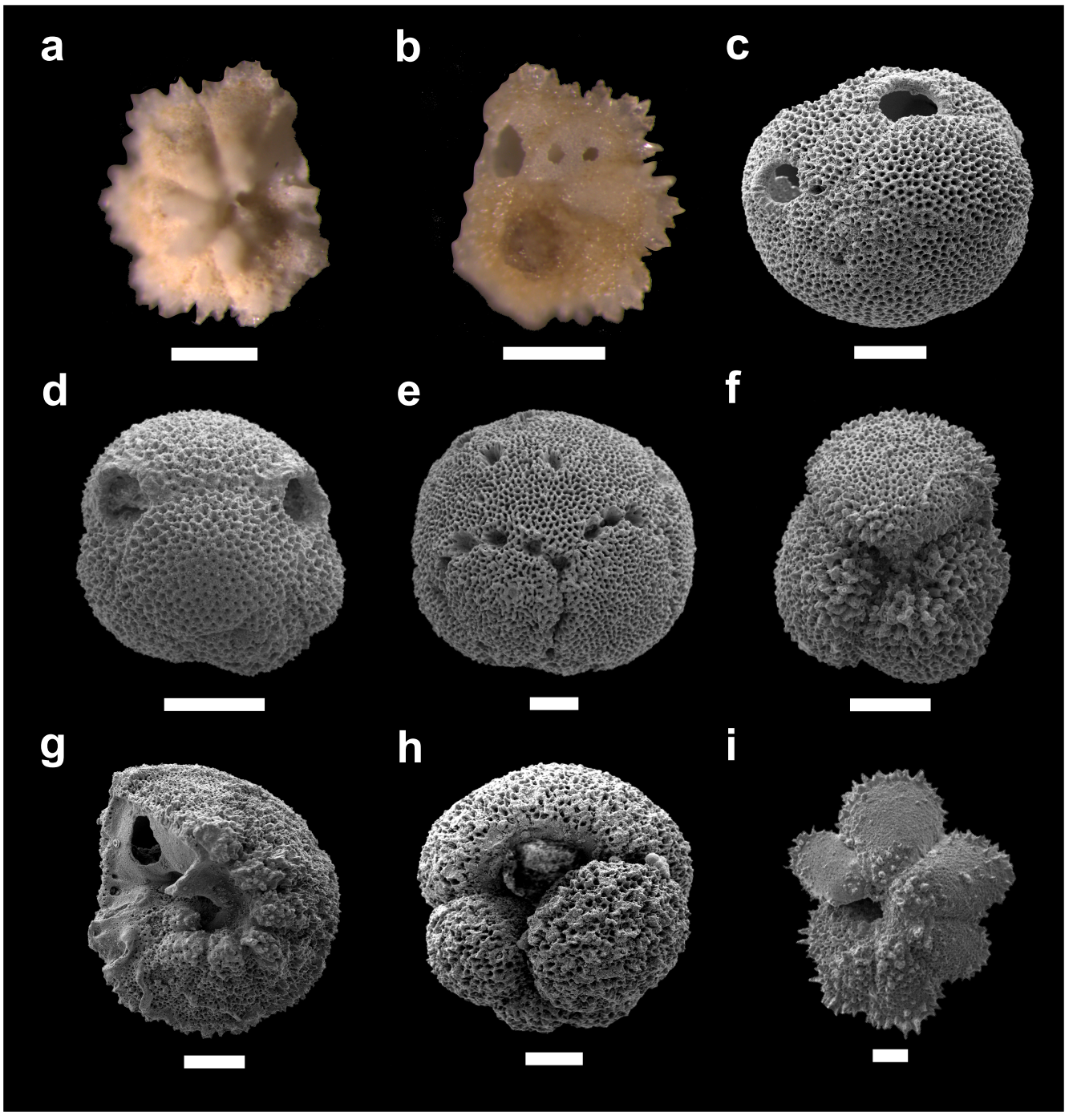
a
b
c
d
e
f
g
h
i

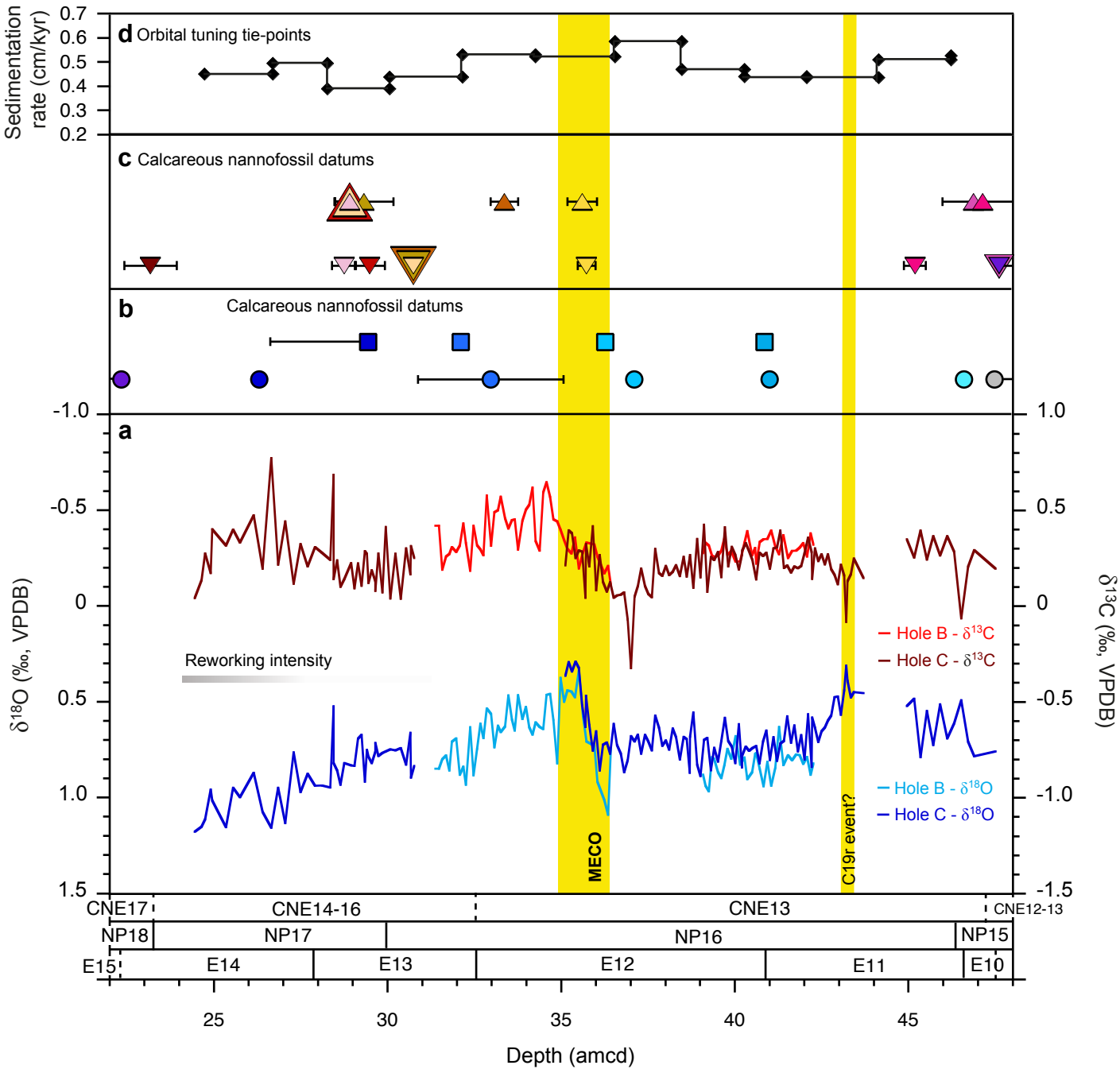


| HOLE B | HOLE C | BIOEVENT |
|---|---|---|
| ▲ | ▼ | B *C. oamaruensis* |
| ▲ | ▼ | T *S. obtusus* |
| ▲ | ▼ | B *R. (D.) bisectus* (>10 μm) |
| ▲ | ▼ | T *C. solitus* |
| ▲ | ▼ | B *R. (D.) scrippsae* (<10 μm) |
| ▲ | ▼ | T *S. furcatolithoides* |
| ▲ | ▼ | B *Cr. reticulatum* |
| ▲ | ▼ | Bc *R. umbilicus* (>14 μm) |
| ▲ | ▼ | T *N. fulgens* |
| ▲ | ▼ | T *C. gigas* |

| HOLE B | HOLE C | BIOEVENT |
|---|---|---|
| ■ | ● | T *G. seminvoluta* |
| ■ | ● | B *G. seminvoluta* |
| ■ | ● | T *O. beckmanni* |
| ■ | ● | B *O. beckmanni* |
| ■ | ● | T *A. bullbrooki* |
| ■ | ● | T *G. nuttalli* |
| ■ | ● | T *M. aragonensis* |
| | | 405 kyr tuning |

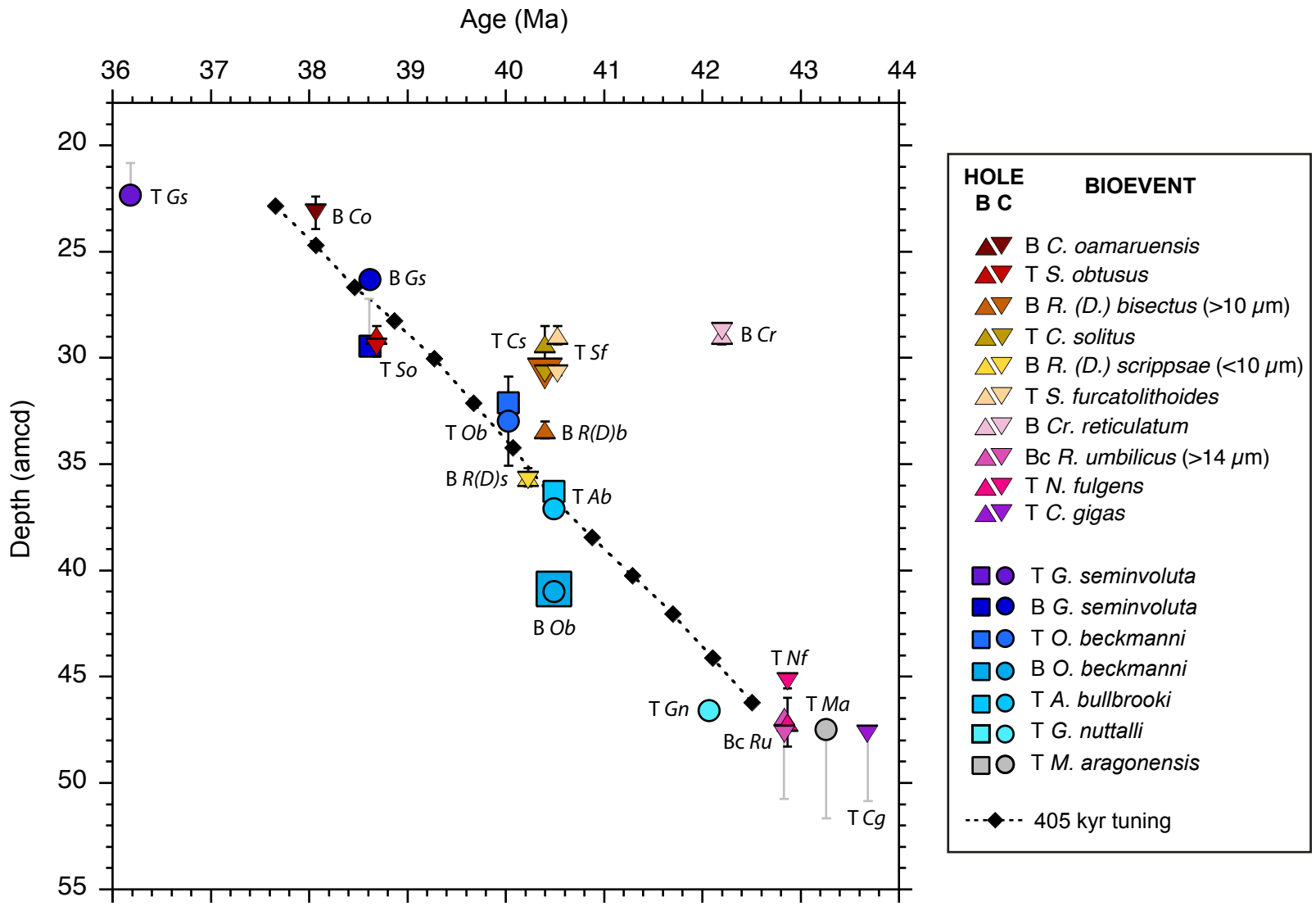
Age (Ma)
36
37
38
39
40
41
42
43
44
Depth (amcd)
20
25
30
35
40
45
50
55
T Gs
B Co
B Gs
T So
T Cs
T Sf
B Cr
T Ob
B R(D)b
B R(D)s
T Ab
B Ob
T Nf
T Gn
T Ma
Bc Ru
T Cg
HOLE
B C
BIOEVENT
B C. oamaruensis
T S. obtusus
B R. (D.) bisectus (>10 μm)
T C. solitus
B R. (D.) scrippsae (<10 μm)
T S. furcatolithoides
B Cr. reticulatum
Bc R. umbilicus (>14 μm)
T N. fulgens
T C. gigas
T G. seminvoluta
B G. seminvoluta
T O. beckmanni
B O. beckmanni
T A. bullbrooki
T G. nuttalli
T M. aragonensis
405 kyr tuning

**Table 1 - Composite depth offsets within splice, ODP Site 865**

| Hole | Core | Splice Offset (m) |
|---|---|---|
| 865B | 4H | 0.78 |
| 865B | 5H | 2.28 |
| 865C | 4H | 0.00 |
| 865C | 5H | 3.22 |
| 865C | 6H | 3.46 |

**Table 2 Splice tie points, ODP Site 865**

| Site, hole, core, section | Interval (cm) | Top of Section Depth (mbsf) | Depth (mbsf) | Splice offset (m) | Depth (mcd) | Correlation | Site, hole, core, section | Interval (cm) | Top of Section Depth (mbsf) | Depth (mbsf) | Splice offset (m) | Depth (mcd) |
|---|---|---|---|---|---|---|---|---|---|---|---|---|
| | | | | | | start=> | 865C-4H-1 | 4 | 22.30 | 22.34 | 0.00 | 22.34 |
| 865C-4H-6 | 20 | 29.80 | 30.00 | 0.00 | 30.00 | tie to: | 865B-4H-2 | 22 | 29.00 | 29.22 | 0.78 | 30.00 |
| 865B-4H-5 | 92 | 33.50 | 34.42 | 0.78 | 35.20 | tie to: | 865C-5H-1 | 18 | 31.80 | 31.98 | 3.22 | 35.20 |
| 865C-5H-5 | 122 | 37.80 | 39.02 | 3.22 | 42.24 | tie to: | 865B-5H-2 | 146 | 38.50 | 39.96 | 2.28 | 42.24 |
| 865B-5H-5 | 44 | 43.00 | 43.44 | 2.28 | 45.72 | tie to: | 865C-6H-1 | 96 | 41.30 | 42.26 | 3.46 | 45.72 |
| 865C-6H-2 | 141 | 42.80 | 44.21 | 3.46 | 47.67 | <=end | | | | | | |

**Table 3 - Mapping pairs for adjusting mcd to amcd, ODP Hole 865B**

| Site-Core-Type | Depth (mcd) | Offset Depth (amcd) |
|---|---|---|
| 865B-4H | 28.40 | 28.44 |
| 865B-4H | 28.90 | 29.02 |
| 865B-4H | 30.00 | 30.00 |
| 865B-4H | 35.20 | 35.20 |
| 865B-4H | 36.21 | 36.32 |
| 865B-5H | 40.12 | 39.82 |
| 865B-5H | 40.50 | 40.30 |
| 865B-5H | 41.32 | 41.20 |
| 865B-5H | 41.74 | 41.72 |
| 865B-5H | 42.24 | 42.24 |
| 865B-5H | 45.72 | 45.72 |
| 865B-5H | 46.80 | 46.81 |

**Table 4 - Mapping pairs for adjusting mcd to amcd, ODP Hole 865C**

| Core | Depth (mcd) | Offset Depth (amcd) |
|---|---|---|
| 865C-4H | 22.30 | 22.30 |
| 865C-4H | 30.00 | 30.00 |
| 865C-4H | 30.42 | 30.64 |
| 865C-5H | 35.20 | 35.20 |
| 865C-5H | 42.24 | 42.24 |
| 865C-5H | 43.84 | 43.74 |
| 865C-6H | 45.06 | 45.12 |
| 865C-6H | 45.72 | 45.72 |
| 865C-6H | 47.67 | 47.67 |

# Table 5. Planktic foraminiferal datums in ODP Holes 865B and C

| Event | Base of planktic foraminiferal Zone | GTS2012 Age (Ma) | Top sample | Top depth (mbsf) | Top depth (mcd) | Top depth (amcd) | Bottom sample | Bottom depth (mbsf) | Bottom depth (mcd) | Bottom depth (amcd) | Mid-point depth (amcd) | ± (m) |
|---|---|---|---|---|---|---|---|---|---|---|---|---|
| **HOLE B** | | | | | | | | | | | | |
| T *G. seminvoluta* | E15 | 36.18 | 3H-2, 75-77 | 20.25 | - | - | 3H-2, 95-97 | 20.45 | - | - | - | - |
| B *G. seminvoluta* | | 38.62 | 3H-6, 110-112 | 26.60 | - | - | 4H-1, 110-112 | 28.62 | 29.40 | 29.47 | - | - |
| T *O. beckmanni* | E13 | 40.03 | 4H-3, 80-82 | 31.30 | 32.08 | 32.08 | 4H-3,W, 90-92 | 31.42 | 32.20 | 32.20 | 32.14 | 0.06 |
| T *A. bullbrooki* | | 40.49 | 4H-CC, 10-12 | 35.36 | 36.14 | 36.24 | 4H-CC, 20-22 | 35.48 | 36.26 | 36.36 | 36.30 | 0.06 |
| B *O. beckmanni* | E12 | 40.49 | 5H-2, 20-22 | 38.70 | 40.98 | 40.83 | 5H-2, 30-32 | 38.82 | 41.10 | 40.96 | 40.89 | 0.07 |
| B *G. index* | | 42.64 | 7H-4, 110-112 | 61.6 | - | - | 7H-5, 55-60 | 62.60 | - | - | - | - |
| B *Mo. lehneri* | | 43.15 | 7H-2, 87-89 | 58.37 | - | - | 7H-3, 57-59 | 59.57 | - | - | - | - |
| T *M. aragonensis* | E10 | 43.26 | 6H-1, 75-77 | 47.25 | - | - | 6H-2,75-77 | 48.77 | - | - | - | - |
| **HOLE C** | | | | | | | | | | | | |
| T *G. seminvoluta* | E15 | 36.18 | 3H-6, 46-48 | 20.76 | 20.76 | - | 4H-1, 5-7 | 22.37 | 22.37 | 22.37 | - | - |
| B *G. seminvoluta* | | 38.62 | 4H-3, 95-97 | 26.25 | 26.25 | 26.25 | 4H-3, 110-112 | 26.42 | 26.42 | 26.42 | 26.34 | 0.07 |
| T *O. beckmanni* | E13 | 40.03 | 4H-CC, 10-12 | 30.7 | 30.7 | 30.91 | 5H-1, 5-7 | 31.87 | 35.09 | 35.10 | 33.00 | 2.10 |
| B *O. beckmanni* | E12 | 40.49 | 5H-4, 145-147 | 37.75 | 40.97 | 40.97 | 5H-5, 5-7 | 37.87 | 41.09 | 41.09 | 41.03 | 0.05 |
| T *A. bullbrooki* | | 40.49 | 5H-2, 55-57 | 33.85 | 37.07 | 37.07 | 5H-2, 65-67 | 33.97 | 37.19 | 37.19 | 37.13 | 0.05 |
| T *Gu. nuttalli* | E11 | 42.07 | 6H-2, 25-27 | 43.05 | 46.51 | 46.51 | 6H-2, 45-47 | 43.27 | 46.73 | 46.73 | 46.62 | 0.10 |
| B *G. index* | | 42.64 | 7H-4, 110-112 | 56.4 | - | - | 7H-5, 70-72 | 57.52 | - | - | - | - |
| B *Mo. lehneri* | | 43.15 | 7H-4, 110-112 | 56.4 | - | - | 7H-5, 70-72 | 57.52 | - | - | - | - |
| T *M. aragonensis* | E10 | 43.26 | 6H-2, 125-127 | 44.05 | 47.51 | 47.51 | 7H-1, 110-112 | 51.92 | - | - | - | - |

T = Top; B = Base; A = *Acarinina;* G = *Globigerinatheka;* Gu = *Guembelitrioides;* M = *Morozovella;* Mo = *Morozovelloides*; O = *Orbulinoides*

Full sample window in which datum could fall is reported, i.e., top depth of top sample and lowermost depth in bottom sample.

**Table 6. Calcareous nannofossil datums in ODP Holes 865B and C**

| Datum | Base of Nannofossil Zone | GTS2012 Age (Ma) | Top sample | Depth (mbsf) | Depth (mcd) | Depth (amcd) | Bottom sample | Depth (mbsf) | Depth (mcd) | Depth (amcd) | Mid point (amcd) | ± (m) |
|---|---|---|---|---|---|---|---|---|---|---|---|---|
| **HOLE B** | | | | | | | | | | | | |
| T *C. grandis* | | **38.01** | 3H-1, 70-72* | 18.70 | - | - | 3H-1, 132* | 19.32 | - | - | - | - |
| B *C. oamaruensis* | NP18 | **38.07** | 3H-3, 110* | 22.10 | - | - | 3H-4, 123* | 23.23 | - | - | - | - |
| T *S. obtusus* | CNE16 | **38.69** | 4H-1, 16* | 27.66 | 28.44 | 28.49 | 4H-2, 40* | 29.40 | 30.18 | 29.35 | 28.92 | 0.43 |
| B R. (*D.) bisectus* (>10 µm) | CNE15 | **40.40** | 4H-4, 20-22 | 32.20 | 32.98 | 32.98 | 4H-4, 107* | 33.07 | 33.85 | 33.76 | 33.37 | 0.39 |
| T *C. solitus* | NP17 | 40.40 | 4H-1, 16* | 27.66 | 28.44 | 28.49 | 4H-2, 40* | 29.4 | 30.18 | 30.18 | 29.33 | 0.85 |
| B R. *(D.) scrippsae* (<10 µm) | | *40.23* | 4H-5, 90-92 | 34.40 | 35.18 | 35.18 | 4H-5, 120* | 34.70 | 35.48 | 36.04 | 35.61 | 0.43 |
| T *S. furcatolithoides* | | **40.53** | 4H-1, 16* | 27.66 | 28.44 | 28.49 | 4H-2, 40* | 29.4 | 30.18 | 29.35 | 28.92 | 0.43 |
| Bc *Cr. reticulatum* | CNE14 | **42.20** | 4H-1, 16* | 27.66 | 28.44 | 28.49 | 4H-2, 40* | 29.40 | 30.18 | 29.35 | 28.92 | 0.43 |
| Bc *R. umbilicus* (>14 µm) | CNE13 | **42.84** | 5H-CC* | 44.58 | 46.86 | 46.87 | 6H-1, 81-85* | 47.35 | - | - | - | - |
| T *N. fulgens* | NP16 | 42.87 | 5H-5, 70-72* | 43.70 | 45.98 | 45.98 | 5H-6, 54-56* | 44.56 | 46.84 | 46.85 | 46.42 | 1.15 |
| B *R. umbilicus* | | 43.32 | 6H-1, 81-85* | 47.31 | - | - | 6H-2, 73-75* | 48.75 | - | - | - | - |
| T *C. gigas* | CNE12; NP15c | **43.68** | 6H-1, 81-85* | 47.31 | - | - | 6H-2, 73-75* | 48.75 | - | - | - | - |
| **HOLE C** | | | | | | | | | | | | |
| T *C. grandis* | | **38.01** | 3H-5, 80* | 18.70 | - | - | 3H-6, 10-11* | 20.41 | - | - | - | - |
| B *C. oamaruensis* | NP18 | **38.07** | 4H-1, 10-11* | 22.40 | 22.40 | 22.40 | 4H-2, 10-11* | 23.91 | 23.91 | 23.91 | 23.15 | 0.76 |
| T *S. obtusus* | CNE16 | **38.69** | 4H-5, 75-77 | 29.05 | 29.05 | 29.05 | 4H-6, 10-11* | 29.91 | 29.91 | 29.91 | 29.48 | 0.43 |
| B R. (*D.) bisectus* (>10 µm) | CNE15 | **40.40** | 4H-6, 65-67 | 30.45 | 30.45 | 30.67 | 4H-CC* | 30.6 | 30.60 | 30.81 | 30.74 | 0.07 |
| T *C. solitus* | NP17 | 40.40 | 4H-6, 65-67 | 30.45 | 30.45 | 30.67 | 4H-CC | 30.6 | 30.60 | 30.81 | 30.74 | 0.07 |
| B R. *(D.) scrippsae* (<10 µm) | | *40.23* | 5H-1, 45-47 | 32.25 | 35.47 | 35.47 | 5H-1, 95-97 | 32.77 | 35.99 | 35.99 | 35.73 | 0.26 |
| T *S. furcatolithoides* | | **40.53** | 4H-6, 65-67 | 30.45 | 30.45 | 30.67 | 4H-CC | 30.6 | 30.60 | 30.81 | 30.74 | 0.07 |
| Bc *Cr. reticulatum* | CNE14 | **42.20** | 4H-5, 10-11* | 28.40 | 28.40 | 28.40 | 4H-5, 75-77 | 29.07 | 29.07 | 29.07 | 28.73 | 0.34 |
| Bc *R. umbilicus* (>14 µm) | CNE13 | **42.84** | 6H-CC* | 44.22 | 47.68 | 47.68 | 7H-1, 10-11* | 50.91 | - | - | - | - |
| T *N. fulgens* | NP16 | 42.87 | 6H-1, 10-11* | 41.40 | 44.86 | 44.89 | 6H-1, 75* | 42.05 | 45.51 | 45.53 | 45.21 | 0.32 |
| B *R. umbilicus* | | 43.32 | 7H-2, 10-11* | 52.40 | - | - | 7H-2, 100* | 53.3 | - | - | - | - |
| T *C. gigas* | CNE12; NP15c | **43.68** | 6H-CC* | 44.22 | 47.68 | 47.68 | 7H-1,10-11* | 50.91 | - | - | - | - |

T = Top; B = Base; C = Chiasmolithus; Cr = Cribrocentrum; D = Dictyococcites; N = Nannotetrina; R = Reticulofenestra; S = Sphenolithus;* = From Bralower and Mutterlose (1995)

All ages on the GTS2012 timescale from Gradstein *et al.* (2012) with those in bold recalculated based on revised calibrations from Agnini *et al.* (2014), in italics from Bohaty *et al.* (2009).

Calcareous nannofossil zones: NP Zones are from Martini (1971) and CNE Zones are from Agnini *et al.* (2014)

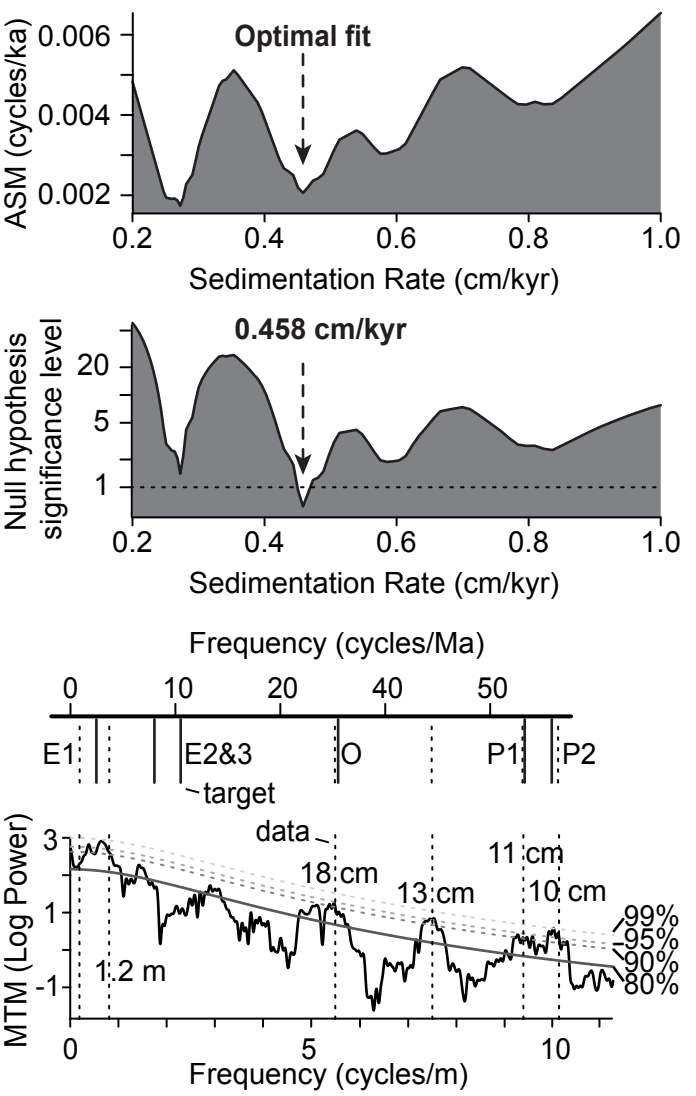
ASM (cycles/ka)
0.006
0.004
0.002
Optimal fit
0.2
0.4
0.6
0.8
1.0
Sedimentation Rate (cm/kyr)
Null hypothesis significance level
20
5
1
0.458 cm/kyr
0.2
0.4
0.6
0.8
1.0
Sedimentation Rate (cm/kyr)
Frequency (cycles/Ma)
0
10
20
40
50
E1
E2&3
O
P1
P2
target
MTM (Log Power)
3
1
-1
data
18 cm
13 cm
11 cm
10 cm
1.2 m
99%
95%
90%
80%
0
5
10
Frequency (cycles/m)

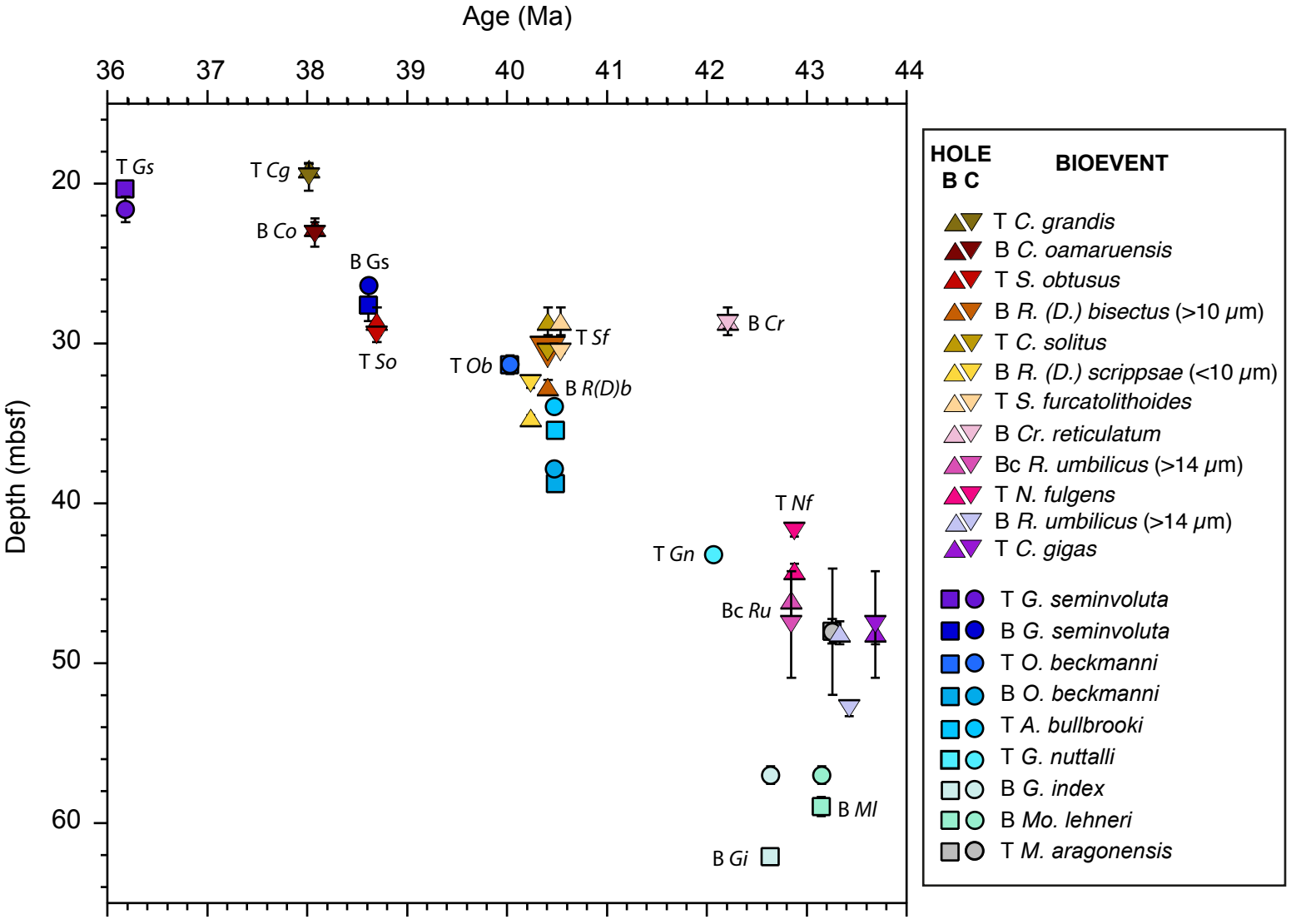
Age (Ma)
36
37
38
39
40
41
42
43
44
Depth (mbsf)
20
30
40
50
60
T Gs
T Cg
B Co
B Gs
T So
T Ob
T Sf
B R(D)b
B Cr
T Nf
T Gn
Bc Ru
B Ml
B Gi
HOLE
B C
BIOEVENT
T C. grandis
B C. oamaruensis
T S. obtusus
B R. (D.) bisectus (>10 µm)
T C. solitus
B R. (D.) scrippsae (<10 µm)
T S. furcatolithoides
B Cr. reticulatum
Bc R. umbilicus (>14 µm)
T N. fulgens
B R. umbilicus (>14 µm)
T C. gigas
T G. seminvoluta
B G. seminvoluta
T O. beckmanni
B O. beckmanni
T A. bullbrooki
T G. nuttalli
B G. index
B Mo. lehneri
T M. aragonensis

## Supplementary Table 2. Benthic foraminifera *Nuttallides truempyi* stable isotope data for ODP Hole 865B from the 250-300 µm sieve size fraction

| Site | Hole | Core | Type | Section | Half | Top (cm) | Bottom (cm) | Depth (mbsf) | Splice offset (m) | Depth (mcd) | Adjusted Composite Depth (amcd) | Orbitally-tuned Age (Ma; GTS2012) | Coarse fraction (>63 µm, %) | δ13C (per mil, VPDB) | δ18O (per mil, VPDB) |
|---|---|---|---|---|---|---|---|---|---|---|---|---|---|---|---|
| 865 | B | 4 | H | 3 | W | 10 | 12 | 30.60 | 0.78 | 31.38 | 31.380 | 39.531 | 35.98 | 0.420 | 0.850 |
| 865 | B | 4 | H | 3 | W | 20 | 22 | 30.70 | 0.78 | 31.48 | 31.480 | 39.550 | 37.07 | 0.420 | 0.850 |
| 865 | B | 4 | H | 3 | W | 30 | 32 | 30.80 | 0.78 | 31.58 | 31.580 | 39.568 | 34.51 | 0.190 | 0.801 |
| 865 | B | 4 | H | 3 | W | 40 | 42 | 30.90 | 0.78 | 31.68 | 31.680 | 39.587 | 32.82 | 0.260 | 0.780 |
| 865 | B | 4 | H | 3 | W | 50 | 52 | 31.00 | 0.78 | 31.78 | 31.780 | 39.606 | 29.66 | 0.273 | 0.859 |
| 865 | B | 4 | H | 3 | W | 58 | 62 | 31.08 | 0.78 | 31.86 | 31.860 | 39.621 | 28.74 | 0.308 | 0.709 |
| 865 | B | 4 | H | 3 | W | 70 | 72 | 31.20 | 0.78 | 31.98 | 31.980 | 39.644 | 30.14 | 0.283 | 0.691 |
| 865 | B | 4 | H | 3 | W | 80 | 82 | 31.30 | 0.78 | 32.08 | 32.080 | 39.663 | 28.64 | 0.316 | 0.881 |
| 865 | B | 4 | H | 3 | W | 90 | 92 | 31.40 | 0.78 | 32.18 | 32.180 | 39.682 | 29.06 | 0.432 | 0.839 |
| 865 | B | 4 | H | 3 | W | 98 | 102 | 31.48 | 0.78 | 32.26 | 32.260 | 39.697 | 31.50 | 0.329 | 0.933 |
| 865 | B | 4 | H | 3 | W | 110 | 112 | 31.60 | 0.78 | 32.38 | 32.380 | 39.720 | 26.40 | 0.185 | 0.634 |
| 865 | B | 4 | H | 3 | W | 120 | 122 | 31.70 | 0.78 | 32.48 | 32.480 | 39.739 | 27.29 | 0.419 | 0.885 |
| 865 | B | 4 | H | 3 | W | 130 | 132 | 31.80 | 0.78 | 32.58 | 32.580 | 39.758 | 32.04 | 0.318 | 0.745 |
| 865 | B | 4 | H | 3 | W | 140 | 142 | 31.90 | 0.78 | 32.68 | 32.680 | 39.777 | 35.03 | 0.296 | 0.615 |
| 865 | B | 4 | H | 3 | W | 148 | 150 | 31.98 | 0.78 | 32.76 | 32.760 | 39.793 | 33.52 | 0.266 | 0.690 |
| 865 | B | 4 | H | 4 | W | 8 | 12 | 32.08 | 0.78 | 32.86 | 32.860 | 39.812 | 32.46 | 0.578 | 0.535 |
| 865 | B | 4 | H | 4 | W | 20 | 22 | 32.20 | 0.78 | 32.98 | 32.980 | 39.835 | 34.05 | 0.315 | 0.564 |
| 865 | B | 4 | H | 4 | W | 30 | 32 | 32.30 | 0.78 | 33.08 | 33.080 | 39.854 | 35.80 | 0.491 | 0.737 |
| 865 | B | 4 | H | 4 | W | 40 | 42 | 32.40 | 0.78 | 33.18 | 33.180 | 39.873 | 34.18 | 0.501 | 0.625 |
| 865 | B | 4 | H | 4 | W | 48 | 50 | 32.48 | 0.78 | 33.26 | 33.260 | 39.888 | 35.82 | 0.571 | 0.658 |
| 865 | B | 4 | H | 4 | W | 60 | 62 | 32.60 | 0.78 | 33.38 | 33.380 | 39.911 | 37.69 | 0.459 | 0.629 |
| 865 | B | 4 | H | 4 | W | 70 | 72 | 32.70 | 0.78 | 33.48 | 33.480 | 39.931 | 32.72 | 0.405 | 0.468 |
| 865 | B | 4 | H | 4 | W | 80 | 82 | 32.80 | 0.78 | 33.58 | 33.580 | 39.950 | 33.91 | 0.450 | 0.594 |
| 865 | B | 4 | H | 4 | W | 88 | 92 | 32.88 | 0.78 | 33.66 | 33.660 | 39.965 | 28.53 | 0.453 | 0.650 |
| 865 | B | 4 | H | 4 | W | 98 | 100 | 32.98 | 0.78 | 33.76 | 33.760 | 39.984 | 28.51 | 0.294 | 0.466 |
| 865 | B | 4 | H | 4 | W | 110 | 112 | 33.10 | 0.78 | 33.88 | 33.880 | 40.007 | 28.66 | 0.445 | 0.591 |
| 865 | B | 4 | H | 4 | W | 120 | 122 | 33.20 | 0.78 | 33.98 | 33.980 | 40.026 | 26.18 | 0.503 | 0.528 |

| | | | | | | | | | | | | | | | |
|---|---|---|---|---|---|---|---|---|---|---|---|---|---|---|---|
| 865 | B | 4 | H | 4 | W | 130 | 132 | 33.30 | 0.78 | 34.08 | 34.080 | 40.045 | 27.00 | 0.528 | 0.633 |
| 865 | B | 4 | H | 4 | W | 140 | 142 | 33.40 | 0.78 | 34.18 | 34.180 | 40.065 | 28.55 | 0.618 | 0.671 |
| 865 | B | 4 | H | 4 | W | 148 | 150 | 33.48 | 0.78 | 34.26 | 34.260 | 40.079 | 27.69 | 0.341 | 0.608 |
| 865 | B | 4 | H | 5 | W | 10 | 12 | 33.60 | 0.78 | 34.38 | 34.380 | 40.100 | 31.31 | 0.289 | 0.631 |
| 865 | B | 4 | H | 5 | W | 20 | 22 | 33.70 | 0.78 | 34.48 | 34.480 | 40.117 | 30.32 | 0.593 | 0.643 |
| 865 | B | 4 | H | 5 | W | 30 | 32 | 33.80 | 0.78 | 34.58 | 34.580 | 40.134 | 27.02 | 0.647 | 0.464 |
| 865 | B | 4 | H | 5 | W | 40 | 42 | 33.90 | 0.78 | 34.68 | 34.680 | 40.151 | 26.59 | 0.570 | 0.459 |
| 865 | B | 4 | H | 5 | W | 50 | 52 | 34.00 | 0.78 | 34.78 | 34.780 | 40.169 | 26.77 | 0.453 | 0.595 |
| 865 | B | 4 | H | 5 | W | 60 | 62 | 34.10 | 0.78 | 34.88 | 34.880 | 40.186 | 28.04 | 0.443 | 0.822 |
| 865 | B | 4 | H | 5 | W | 70 | 72 | 34.20 | 0.78 | 34.98 | 34.980 | 40.203 | 26.37 | 0.398 | 0.376 |
| 865 | B | 4 | H | 5 | W | 80 | 82 | 34.30 | 0.78 | 35.08 | 35.080 | 40.220 | 32.21 | 0.345 | 0.500 |
| 865 | B | 4 | H | 5 | W | 90 | 92 | 34.40 | 0.78 | 35.18 | 35.180 | 40.237 | 28.22 | 0.299 | 0.441 |
| 865 | B | 4 | H | 5 | W | 100 | 104 | 34.50 | 0.78 | 35.28 | 35.289 | 40.256 | 25.93 | 0.276 | 0.446 |
| 865 | B | 4 | H | 5 | W | 110 | 112 | 34.60 | 0.78 | 35.38 | 35.400 | 40.275 | 24.41 | 0.359 | 0.476 |
| 865 | B | 4 | H | 5 | W | 120 | 122 | 34.70 | 0.78 | 35.48 | 35.510 | 40.294 | 23.85 | 0.197 | 0.338 |
| 865 | B | 4 | H | 5 | W | 130 | 132 | 34.80 | 0.78 | 35.58 | 35.621 | 40.313 | 23.05 | 0.278 | 0.571 |
| 865 | B | 4 | H | 5 | W | 140 | 142 | 34.90 | 0.78 | 35.68 | 35.732 | 40.332 | 25.94 | 0.333 | 0.708 |
| 865 | B | 4 | H | 6 | W | 10 | 12 | 35.10 | 0.78 | 35.88 | 35.954 | 40.370 | 23.94 | 0.321 | 0.730 |
| 865 | B | 4 | H | 6 | W | 18 | 20 | 35.18 | 0.78 | 35.96 | 36.043 | 40.385 | 21.21 | 0.259 | 0.917 |
| 865 | B | 4 | H | CC | W | 10 | 12 | 35.36 | 0.78 | 36.14 | 36.242 | 40.419 | 20.39 | 0.171 | 1.013 |
| 865 | B | 4 | H | CC | W | 20 | 22 | 35.46 | 0.78 | 36.24 | 36.347 | 40.437 | 19.73 | 0.210 | 1.090 |
| 865 | B | 4 | H | CC | W | 30 | 32 | 35.56 | 0.78 | 36.34 | 36.436 | 40.452 | 21.12 | 0.110 | 0.742 |
| 865 | B | 5 | H | 1 | W | 2 | 4 | 37.02 | 2.28 | 39.30 | 39.086 | 41.022 | 16.64 | 0.277 | 0.879 |
| 865 | B | 5 | H | 1 | W | 10 | 12 | 37.10 | 2.28 | 39.38 | 39.158 | 41.038 | 17.95 | 0.330 | 0.938 |
| 865 | B | 5 | H | 1 | W | 20 | 22 | 37.20 | 2.28 | 39.48 | 39.247 | 41.058 | 17.02 | 0.316 | 0.968 |
| 865 | B | 5 | H | 1 | W | 30 | 32 | 37.30 | 2.28 | 39.58 | 39.337 | 41.079 | 17.19 | 0.264 | 0.790 |
| 865 | B | 5 | H | 1 | W | 38 | 40 | 37.38 | 2.28 | 39.66 | 39.408 | 41.095 | 17.61 | 0.257 | 0.799 |
| 865 | B | 5 | H | 1 | W | 50 | 52 | 37.50 | 2.28 | 39.78 | 39.516 | 41.119 | 16.19 | 0.263 | 0.869 |
| 865 | B | 5 | H | 1 | W | 60 | 62 | 37.60 | 2.28 | 39.88 | 39.605 | 41.140 | 18.57 | 0.290 | 0.898 |
| 865 | B | 5 | H | 1 | W | 70 | 72 | 37.70 | 2.28 | 39.98 | 39.695 | 41.160 | 17.32 | 0.355 | 0.831 |
| 865 | B | 5 | H | 1 | W | 80 | 82 | 37.80 | 2.28 | 40.08 | 39.784 | 41.181 | 19.40 | 0.269 | 0.745 |
| 865 | B | 5 | H | 1 | W | 90 | 92 | 37.90 | 2.28 | 40.18 | 39.896 | 41.206 | 16.47 | 0.286 | 0.797 |
| 865 | B | 5 | H | 1 | W | 100 | 104 | 38.00 | 2.28 | 40.28 | 40.022 | 41.235 | 20.05 | 0.233 | 0.679 |
| 865 | B | 5 | H | 1 | W | 110 | 112 | 38.10 | 2.28 | 40.38 | 40.148 | 41.264 | 16.20 | 0.235 | 0.828 |
| 865 | B | 5 | H | 1 | W | 120 | 122 | 38.20 | 2.28 | 40.48 | 40.275 | 41.292 | 15.65 | 0.330 | 0.792 |
| 865 | B | 5 | H | 1 | W | 127 | 129 | 38.27 | 2.28 | 40.55 | 40.355 | 41.311 | 17.22 | 0.392 | 0.904 |
| 865 | B | 5 | H | 1 | W | 140 | 142 | 38.40 | 2.28 | 40.68 | 40.498 | 41.344 | 16.52 | 0.266 | 0.869 |

| | | | | | | | | | | | | | | | |
|---|---|---|---|---|---|---|---|---|---|---|---|---|---|---|---|
| 865 | B | 5 | H | 1 | W | 148 | 150 | 38.48 | 2.28 | 40.76 | 40.585 | 41.364 | 15.34 | 0.304 | 0.772 |
| 865 | B | 5 | H | 2 | W | 0 | 2 | 38.50 | 2.28 | 40.78 | 40.607 | 41.369 | 13.69 | 0.221 | 0.769 |
| 865 | B | 5 | H | 2 | W | 10 | 12 | 38.60 | 2.28 | 40.88 | 40.717 | 41.394 | 13.56 | 0.335 | 0.851 |
| 865 | B | 5 | H | 2 | W | 20 | 22 | 38.70 | 2.28 | 40.98 | 40.827 | 41.419 | 12.14 | 0.350 | 0.942 |
| 865 | B | 5 | H | 2 | W | 30 | 32 | 38.80 | 2.28 | 41.08 | 40.937 | 41.445 | 13.51 | 0.351 | 0.813 |
| 865 | B | 5 | H | 2 | W | 40 | 42 | 38.90 | 2.28 | 41.18 | 41.046 | 41.470 | 13.57 | 0.394 | 0.938 |
| 865 | B | 5 | H | 2 | W | 50 | 52 | 39.00 | 2.28 | 41.28 | 41.156 | 41.495 | 12.28 | 0.311 | 0.845 |
| 865 | B | 5 | H | 2 | W | 60 | 62 | 39.10 | 2.28 | 41.38 | 41.274 | 41.522 | 13.51 | 0.270 | 0.631 |
| 865 | B | 5 | H | 2 | W | 70 | 72 | 39.20 | 2.28 | 41.48 | 41.398 | 41.551 | 12.30 | 0.371 | 0.830 |
| 865 | B | 5 | H | 2 | W | 80 | 82 | 39.30 | 2.28 | 41.58 | 41.522 | 41.579 | 13.61 | 0.252 | 0.778 |
| 865 | B | 5 | H | 2 | W | 90 | 92 | 39.40 | 2.28 | 41.68 | 41.646 | 41.608 | 13.82 | 0.288 | 0.805 |
| 865 | B | 5 | H | 2 | W | 100 | 104 | 39.50 | 2.28 | 41.78 | 41.762 | 41.634 | 15.22 | 0.290 | 0.775 |
| 865 | B | 5 | H | 2 | W | 110 | 112 | 39.60 | 2.28 | 41.88 | 41.866 | 41.658 | 11.80 | 0.305 | 0.778 |
| 865 | B | 5 | H | 2 | W | 120 | 122 | 39.70 | 2.28 | 41.98 | 41.970 | 41.682 | 14.29 | 0.329 | 0.824 |
| 865 | B | 5 | H | 2 | W | 130 | 132 | 39.80 | 2.28 | 42.08 | 42.074 | 41.706 | 14.11 | 0.259 | 0.788 |
| 865 | B | 5 | H | 2 | W | 140 | 142 | 39.90 | 2.28 | 42.18 | 42.178 | 41.726 | 11.64 | 0.379 | 0.881 |
| 865 | B | 5 | H | 2 | W | 148 | 150 | 39.98 | 2.28 | 42.26 | 42.260 | 41.742 | 11.29 | 0.319 | 0.821 |

## Supplementary Table 3. Benthic foraminifera *Nuttallides truempyi* stable isotope data for ODP Hole 865C from the 250-300 µm sieve size fraction

| Site | Hole | Core | Type | Section | Half | Top (cm) | Bottom (cm) | Depth (mbsf) | Splice offset (m) | Depth (mcd) | Adjusted Composite Depth (amcd) | Orbitally-tuned Age (Ma; GTS2012) | Coarse fraction (>63 µm, %) | δ13C (per mil, VPDB) | δ18O (per mil, VPDB) |
|---|---|---|---|---|---|---|---|---|---|---|---|---|---|---|---|
| 865 | C | 4 | H | 2 | W | 65 | 67 | 24.45 | 0.00 | 24.45 | 24.450 | 38.010 | 11.35 | 0.042 | 1.179 |
| 865 | C | 4 | H | 2 | W | 85 | 87 | 24.65 | 0.00 | 24.65 | 24.650 | 38.054 | 12.95 | 0.136 | 1.151 |
| 865 | C | 4 | H | 2 | W | 95 | 97 | 24.75 | 0.00 | 24.75 | 24.750 | 38.076 | 11.01 | 0.275 | 1.114 |
| 865 | C | 4 | H | 2 | W | 110 | 112 | 24.91 | 0.00 | 24.91 | 24.910 | 38.108 | - | 0.172 | 0.959 |
| 865 | C | 4 | H | 2 | W | 115 | 117 | 24.95 | 0.00 | 24.95 | 24.950 | 38.116 | 13.23 | 0.402 | 1.015 |
| 865 | C | 4 | H | 3 | W | 5 | 7 | 25.35 | 0.00 | 25.35 | 25.350 | 38.197 | 20.08 | 0.317 | 1.155 |
| 865 | C | 4 | H | 3 | W | 25 | 27 | 25.55 | 0.00 | 25.55 | 25.550 | 38.238 | 14.70 | 0.401 | 0.950 |
| 865 | C | 4 | H | 3 | W | 45 | 47 | 25.75 | 0.00 | 25.75 | 25.750 | 38.278 | 13.69 | 0.333 | 0.998 |
| 865 | C | 4 | H | 3 | W | 85 | 87 | 26.15 | 0.00 | 26.15 | 26.150 | 38.359 | 12.85 | 0.475 | 0.870 |
| 865 | C | 4 | H | 3 | W | 110 | 112 | 26.41 | 0.00 | 26.41 | 26.410 | 38.411 | - | 0.195 | 1.075 |
| 865 | C | 4 | H | 3 | W | 135 | 137 | 26.65 | 0.00 | 26.65 | 26.650 | 38.460 | 14.28 | 0.773 | 1.158 |
| 865 | C | 4 | H | 4 | W | 5 | 7 | 26.85 | 0.00 | 26.85 | 26.850 | 38.510 | 13.05 | 0.217 | 0.949 |
| 865 | C | 4 | H | 4 | W | 25 | 27 | 27.05 | 0.00 | 27.05 | 27.050 | 38.561 | 16.67 | 0.443 | 1.134 |
| 865 | C | 4 | H | 4 | W | 50 | 52 | 27.30 | 0.00 | 27.30 | 27.300 | 38.625 | 18.64 | 0.118 | 0.764 |
| 865 | C | 4 | H | 4 | W | 70 | 72 | 27.50 | 0.00 | 27.50 | 27.500 | 38.676 | 19.94 | 0.324 | 0.972 |
| 865 | C | 4 | H | 4 | W | 90 | 92 | 27.70 | 0.00 | 27.70 | 27.700 | 38.727 | 20.82 | 0.208 | 0.876 |
| 865 | C | 4 | H | 4 | W | 112 | 114 | 27.92 | 0.00 | 27.92 | 27.920 | 38.784 | 22.34 | 0.309 | 0.938 |
| 865 | C | 4 | H | 4 | W | 131 | 133 | 28.11 | 0.00 | 28.11 | 28.110 | 38.833 | 19.61 | 0.279 | 0.937 |
| 865 | C | 4 | H | 5 | W | 5 | 7 | 28.35 | 0.00 | 28.35 | 28.350 | 38.892 | 30.63 | 0.243 | 0.948 |
| 865 | C | 4 | H | 5 | W | 15 | 17 | 28.45 | 0.00 | 28.45 | 28.450 | 38.914 | 19.73 | 0.684 | 0.524 |
| 865 | C | 4 | H | 5 | W | 15 | 17 | 28.45 | 0.00 | 28.45 | 28.450 | 38.914 | - | 0.141 | 0.820 |
| 865 | C | 4 | H | 5 | W | 25 | 27 | 28.55 | 0.00 | 28.55 | 28.550 | 38.937 | 27.04 | 0.239 | 0.859 |

| | | | | | | | | | | | | | | | |
|---|---|---|---|---|---|---|---|---|---|---|---|---|---|---|---|
| 865 | C | 4 | H | 5 | W | 35 | 37 | 28.65 | 0.00 | 28.65 | 28.650 | 38.960 | 25.99 | 0.101 | 0.933 |
| 865 | C | 4 | H | 5 | W | 45 | 47 | 28.75 | 0.00 | 28.75 | 28.750 | 38.983 | 27.30 | 0.141 | 0.820 |
| 865 | C | 4 | H | 5 | W | 65 | 67 | 28.95 | 0.00 | 28.95 | 28.950 | 39.029 | 24.10 | 0.225 | 0.833 |
| 865 | C | 4 | H | 5 | W | 75 | 77 | 29.05 | 0.00 | 29.05 | 29.050 | 39.052 | 25.44 | 0.094 | 0.835 |
| 865 | C | 4 | H | 5 | W | 85 | 87 | 29.15 | 0.00 | 29.15 | 29.150 | 39.075 | 19.99 | 0.223 | 0.694 |
| 865 | C | 4 | H | 5 | W | 95 | 97 | 29.25 | 0.00 | 29.25 | 29.250 | 39.097 | 24.35 | 0.106 | 0.673 |
| 865 | C | 4 | H | 5 | W | 105 | 107 | 29.35 | 0.00 | 29.35 | 29.350 | 39.120 | 26.16 | 0.286 | 0.918 |
| 865 | C | 4 | H | 5 | W | 110 | 112 | 29.41 | 0.00 | 29.41 | 29.410 | 39.134 | - | 0.272 | 0.752 |
| 865 | C | 4 | H | 5 | W | 115 | 117 | 29.45 | 0.00 | 29.45 | 29.450 | 39.143 | 24.27 | 0.120 | 0.787 |
| 865 | C | 4 | H | 5 | W | 125 | 127 | 29.55 | 0.00 | 29.55 | 29.550 | 39.166 | 26.11 | 0.187 | 0.819 |
| 865 | C | 4 | H | 5 | W | 135 | 137 | 29.65 | 0.00 | 29.65 | 29.650 | 39.189 | 25.38 | 0.130 | 0.762 |
| 865 | C | 4 | H | 5 | W | 135 | 137 | 29.65 | 0.00 | 29.65 | 29.650 | 39.189 | 25.38 | 0.079 | 0.716 |
| 865 | C | 4 | H | 5 | W | 144 | 146 | 29.74 | 0.00 | 29.74 | 29.740 | 39.209 | 28.65 | 0.275 | 0.783 |
| 865 | C | 4 | H | 6 | W | 5 | 7 | 29.85 | 0.00 | 29.85 | 29.850 | 39.235 | 25.64 | 0.072 | 0.767 |
| 865 | C | 4 | H | 6 | W | 15 | 17 | 29.95 | 0.00 | 29.95 | 29.950 | 39.257 | 20.96 | 0.413 | 0.760 |
| 865 | C | 4 | H | 6 | W | 25 | 27 | 30.05 | 0.00 | 30.05 | 30.076 | 39.285 | 24.03 | 0.040 | 0.749 |
| 865 | C | 4 | H | 6 | W | 35 | 37 | 30.15 | 0.00 | 30.15 | 30.229 | 39.314 | 26.28 | 0.274 | 0.753 |
| 865 | C | 4 | H | 6 | W | 45 | 47 | 30.25 | 0.00 | 30.25 | 30.381 | 39.342 | 23.63 | 0.039 | 0.743 |
| 865 | C | 4 | H | 6 | W | 55 | 57 | 30.35 | 0.00 | 30.35 | 30.533 | 39.371 | 23.94 | 0.302 | 0.827 |
| 865 | C | 4 | H | 6 | W | 63 | 65 | 30.44 | 0.00 | 30.44 | 30.659 | 39.395 | - | 0.166 | 0.661 |
| 865 | C | 4 | H | 6 | W | 65 | 67 | 30.45 | 0.00 | 30.45 | 30.669 | 39.397 | 28.23 | 0.313 | 0.895 |
| 865 | C | 4 | H | 6 | W | 75 | 77 | 30.55 | 0.00 | 30.55 | 30.764 | 39.415 | 34.14 | 0.251 | 0.835 |
| 865 | C | 5 | H | 1 | W | 5 | 7 | 31.85 | 3.22 | 35.07 | 35.076 | 40.219 | 25.71 | 0.213 | 0.365 |
| 865 | C | 5 | H | 1 | W | 15 | 17 | 31.95 | 3.22 | 35.17 | 35.171 | 40.236 | 28.98 | 0.395 | 0.294 |
| 865 | C | 5 | H | 1 | W | 25 | 27 | 32.05 | 3.22 | 35.27 | 35.270 | 40.252 | 24.04 | 0.380 | 0.343 |
| 865 | C | 5 | H | 1 | W | 35 | 37 | 32.15 | 3.22 | 35.37 | 35.370 | 40.270 | 17.04 | 0.252 | 0.290 |
| 865 | C | 5 | H | 1 | W | 45 | 47 | 32.25 | 3.22 | 35.47 | 35.470 | 40.287 | 21.30 | 0.292 | 0.324 |
| 865 | C | 5 | H | 1 | W | 55 | 57 | 32.35 | 3.22 | 35.57 | 35.570 | 40.304 | 17.34 | 0.285 | 0.520 |
| 865 | C | 5 | H | 1 | W | 63 | 65 | 32.44 | 3.22 | 35.66 | 35.660 | 40.319 | - | 0.044 | 0.632 |

| | | | | | | | | | | | | | | | |
|---|---|---|---|---|---|---|---|---|---|---|---|---|---|---|---|
| 865 | C | 5 | H | 1 | W | 65 | 67 | 32.45 | 3.22 | 35.67 | 35.670 | 40.321 | 21.74 | 0.325 | 0.469 |
| 865 | C | 5 | H | 1 | W | 75 | 77 | 32.55 | 3.22 | 35.77 | 35.770 | 40.338 | 19.14 | 0.207 | 0.621 |
| 865 | C | 5 | H | 1 | W | 85 | 87 | 32.65 | 3.22 | 35.87 | 35.870 | 40.355 | 24.03 | 0.417 | 0.755 |
| 865 | C | 5 | H | 1 | W | 95 | 97 | 32.75 | 3.22 | 35.97 | 35.970 | 40.372 | 19.13 | 0.082 | 0.653 |
| 865 | C | 5 | H | 1 | W | 105 | 107 | 32.85 | 3.22 | 36.07 | 36.070 | 40.389 | 19.62 | 0.268 | 0.859 |
| 865 | C | 5 | H | 1 | W | 115 | 117 | 32.95 | 3.22 | 36.17 | 36.170 | 40.407 | 15.61 | 0.127 | 0.725 |
| 865 | C | 5 | H | 1 | W | 125 | 127 | 33.05 | 3.22 | 36.27 | 36.270 | 40.424 | 14.59 | 0.076 | 0.712 |
| 865 | C | 5 | H | 1 | W | 135 | 137 | 33.15 | 3.22 | 36.37 | 36.370 | 40.441 | 15.48 | 0.125 | 0.770 |
| 865 | C | 5 | H | 1 | W | 145 | 147 | 33.25 | 3.22 | 36.47 | 36.470 | 40.458 | 15.11 | 0.045 | 0.616 |
| 865 | C | 5 | H | 2 | W | 5 | 7 | 33.35 | 3.22 | 36.57 | 36.570 | 40.476 | 13.47 | 0.055 | 0.727 |
| 865 | C | 5 | H | 2 | W | 15 | 17 | 33.45 | 3.22 | 36.67 | 36.670 | 40.498 | 17.54 | 0.060 | 0.771 |
| 865 | C | 5 | H | 2 | W | 25 | 27 | 33.55 | 3.22 | 36.77 | 36.770 | 40.519 | 13.46 | 0.072 | 0.869 |
| 865 | C | 5 | H | 2 | W | 35 | 37 | 33.65 | 3.22 | 36.87 | 36.870 | 40.540 | 15.43 | -0.070 | 0.806 |
| 865 | C | 5 | H | 2 | W | 45 | 47 | 33.75 | 3.22 | 36.97 | 36.970 | 40.562 | 11.93 | -0.324 | 0.679 |
| 865 | C | 5 | H | 2 | W | 55 | 57 | 33.85 | 3.22 | 37.07 | 37.070 | 40.583 | 16.03 | 0.050 | 0.707 |
| 865 | C | 5 | H | 2 | W | 65 | 67 | 33.95 | 3.22 | 37.17 | 37.170 | 40.604 | 13.65 | 0.105 | 0.671 |
| 865 | C | 5 | H | 2 | W | 75 | 77 | 34.05 | 3.22 | 37.27 | 37.270 | 40.626 | 17.29 | 0.196 | 0.770 |
| 865 | C | 5 | H | 2 | W | 85 | 87 | 34.15 | 3.22 | 37.37 | 37.370 | 40.647 | 14.06 | 0.104 | 0.673 |
| 865 | C | 5 | H | 2 | W | 95 | 97 | 34.25 | 3.22 | 37.47 | 37.470 | 40.668 | 16.85 | 0.064 | 0.707 |
| 865 | C | 5 | H | 2 | W | 105 | 107 | 34.35 | 3.22 | 37.57 | 37.570 | 40.689 | 13.05 | 0.046 | 0.753 |
| 865 | C | 5 | H | 2 | W | 115 | 117 | 34.45 | 3.22 | 37.67 | 37.670 | 40.711 | 17.56 | 0.299 | 0.572 |
| 865 | C | 5 | H | 2 | W | 125 | 127 | 34.55 | 3.22 | 37.77 | 37.770 | 40.732 | 14.57 | 0.172 | 0.637 |
| 865 | C | 5 | H | 2 | W | 135 | 137 | 34.65 | 3.22 | 37.87 | 37.870 | 40.753 | 16.85 | 0.159 | 0.729 |
| 865 | C | 5 | H | 2 | W | 145 | 147 | 34.75 | 3.22 | 37.97 | 37.970 | 40.775 | 13.95 | 0.210 | 0.702 |
| 865 | C | 5 | H | 3 | W | 5 | 7 | 34.85 | 3.22 | 38.07 | 38.07 | 40.796 | 18.25 | 0.161 | 0.750 |
| 865 | C | 5 | H | 3 | W | 15 | 17 | 34.95 | 3.22 | 38.17 | 38.170 | 40.817 | 12.37 | 0.179 | 0.639 |
| 865 | C | 5 | H | 3 | W | 25 | 27 | 35.05 | 3.22 | 38.27 | 38.270 | 40.839 | 15.74 | 0.214 | 0.685 |
| 865 | C | 5 | H | 3 | W | 35 | 37 | 35.15 | 3.22 | 38.37 | 38.370 | 40.860 | 12.88 | 0.157 | 0.803 |
| 865 | C | 5 | H | 3 | W | 47 | 49 | 35.27 | 3.22 | 38.49 | 38.490 | 40.886 | 17.06 | 0.258 | 0.684 |

| | | | | | | | | | | | | | | | |
|---|---|---|---|---|---|---|---|---|---|---|---|---|---|---|---|
| 865 | C | 5 | H | 3 | W | 55 | 57 | 35.35 | 3.22 | 38.57 | 38.570 | 40.904 | 13.12 | 0.153 | 0.695 |
| 865 | C | 5 | H | 3 | W | 63 | 65 | 35.44 | 3.22 | 38.66 | 38.660 | 40.925 | - | 0.255 | 0.871 |
| 865 | C | 5 | H | 3 | W | 65 | 67 | 35.45 | 3.22 | 38.67 | 38.670 | 40.927 | 16.06 | 0.267 | 0.683 |
| 865 | C | 5 | H | 3 | W | 75 | 77 | 35.55 | 3.22 | 38.77 | 38.770 | 40.950 | 14.32 | 0.096 | 0.555 |
| 865 | C | 5 | H | 3 | W | 85 | 87 | 35.65 | 3.22 | 38.87 | 38.870 | 40.972 | 16.11 | 0.352 | 0.827 |
| 865 | C | 5 | H | 3 | W | 95 | 97 | 35.75 | 3.22 | 38.97 | 38.970 | 40.995 | 14.07 | 0.151 | 0.887 |
| 865 | C | 5 | H | 3 | W | 105 | 107 | 35.85 | 3.22 | 39.07 | 39.070 | 41.018 | 17.51 | 0.425 | 0.700 |
| 865 | C | 5 | H | 3 | W | 115 | 117 | 35.95 | 3.22 | 39.17 | 39.170 | 41.041 | 14.98 | 0.075 | 0.689 |
| 865 | C | 5 | H | 3 | W | 125 | 127 | 36.05 | 3.22 | 39.27 | 39.270 | 41.063 | 16.69 | 0.257 | 0.857 |
| 865 | C | 5 | H | 3 | W | 135 | 137 | 36.15 | 3.22 | 39.37 | 39.370 | 41.086 | 13.98 | 0.241 | 0.741 |
| 865 | C | 5 | H | 3 | W | 145 | 147 | 36.25 | 3.22 | 39.47 | 39.470 | 41.109 | 16.83 | 0.284 | 0.812 |
| 865 | C | 5 | H | 4 | W | 5 | 7 | 36.35 | 3.22 | 39.57 | 39.570 | 41.132 | 14.81 | 0.152 | 0.705 |
| 865 | C | 5 | H | 4 | W | 15 | 17 | 36.45 | 3.22 | 39.67 | 39.670 | 41.155 | 19.05 | 0.412 | 0.585 |
| 865 | C | 5 | H | 4 | W | 25 | 27 | 36.55 | 3.22 | 39.77 | 39.770 | 41.177 | 15.65 | 0.208 | 0.704 |
| 865 | C | 5 | H | 4 | W | 35 | 37 | 36.65 | 3.22 | 39.87 | 39.870 | 41.200 | 18.26 | 0.310 | 0.734 |
| 865 | C | 5 | H | 4 | W | 45 | 47 | 36.75 | 3.22 | 39.97 | 39.970 | 41.223 | 13.12 | 0.267 | 0.820 |
| 865 | C | 5 | H | 4 | W | 55 | 57 | 36.85 | 3.22 | 40.07 | 40.070 | 41.246 | 15.50 | 0.191 | 0.618 |
| 865 | C | 5 | H | 4 | W | 63 | 65 | 36.94 | 3.22 | 40.16 | 40.160 | 41.266 | - | 0.269 | 0.843 |
| 865 | C | 5 | H | 4 | W | 65 | 67 | 36.95 | 3.22 | 40.17 | 40.170 | 41.269 | 12.97 | 0.290 | 0.780 |
| 865 | C | 5 | H | 4 | W | 75 | 77 | 37.05 | 3.22 | 40.27 | 40.270 | 41.291 | 16.16 | 0.329 | 0.735 |
| 865 | C | 5 | H | 4 | W | 85 | 87 | 37.15 | 3.22 | 40.37 | 40.370 | 41.314 | 14.40 | 0.287 | 0.757 |
| 865 | C | 5 | H | 4 | W | 95 | 97 | 37.25 | 3.22 | 40.47 | 40.470 | 41.337 | 14.32 | 0.243 | 0.743 |
| 865 | C | 5 | H | 4 | W | 105 | 107 | 37.35 | 3.22 | 40.57 | 40.570 | 41.360 | 12.31 | 0.140 | 0.731 |
| 865 | C | 5 | H | 4 | W | 115 | 117 | 37.45 | 3.22 | 40.67 | 40.670 | 41.383 | 13.72 | 0.279 | 0.821 |
| 865 | C | 5 | H | 4 | W | 125 | 127 | 37.55 | 3.22 | 40.77 | 40.770 | 41.406 | 11.35 | 0.262 | 0.708 |
| 865 | C | 5 | H | 4 | W | 135 | 137 | 37.65 | 3.22 | 40.87 | 40.870 | 41.429 | 16.01 | 0.278 | 0.651 |
| 865 | C | 5 | H | 4 | W | 145 | 147 | 37.75 | 3.22 | 40.97 | 40.970 | 41.452 | 11.96 | 0.195 | 0.804 |
| 865 | C | 5 | H | 5 | W | 5 | 7 | 37.85 | 3.22 | 41.07 | 41.070 | 41.475 | 20.61 | 0.303 | 0.686 |
| 865 | C | 5 | H | 5 | W | 15 | 17 | 37.95 | 3.22 | 41.17 | 41.170 | 41.498 | 12.77 | 0.307 | 0.809 |

| | | | | | | | | | | | | | | | |
|---|---|---|---|---|---|---|---|---|---|---|---|---|---|---|---|
| 865 | C | 5 | H | 5 | W | 25 | 27 | 38.05 | 3.22 | 41.27 | 41.270 | 41.521 | 19.35 | 0.394 | 0.718 |
| 865 | C | 5 | H | 5 | W | 35 | 37 | 38.15 | 3.22 | 41.37 | 41.370 | 41.544 | 12.29 | 0.200 | 0.705 |
| 865 | C | 5 | H | 5 | W | 45 | 47 | 38.25 | 3.22 | 41.47 | 41.470 | 41.567 | 18.22 | 0.213 | 0.577 |
| 865 | C | 5 | H | 5 | W | 55 | 57 | 38.35 | 3.22 | 41.57 | 41.570 | 41.590 | 12.97 | 0.176 | 0.714 |
| 865 | C | 5 | H | 5 | W | 65 | 67 | 38.45 | 3.22 | 41.67 | 41.670 | 41.613 | 19.39 | 0.208 | 0.623 |
| 865 | C | 5 | H | 5 | W | 75 | 77 | 38.55 | 3.22 | 41.77 | 41.770 | 41.636 | 14.31 | 0.198 | 0.760 |
| 865 | C | 5 | H | 5 | W | 85 | 87 | 38.65 | 3.22 | 41.87 | 41.870 | 41.659 | 18.95 | 0.211 | 0.675 |
| 865 | C | 5 | H | 5 | W | 95 | 97 | 38.75 | 3.22 | 41.97 | 41.970 | 41.682 | 14.08 | 0.277 | 0.802 |
| 865 | C | 5 | H | 5 | W | 105 | 107 | 38.85 | 3.22 | 42.07 | 42.070 | 41.705 | 18.41 | 0.357 | 0.565 |
| 865 | C | 5 | H | 5 | W | 113 | 116 | 38.95 | 3.22 | 42.17 | 42.165 | 41.724 | 10.54 | 0.281 | 0.840 |
| 865 | C | 5 | H | 5 | W | 115 | 117 | 38.96 | 3.22 | 42.18 | 42.180 | 41.727 | 10.73 | 0.142 | 0.583 |
| 865 | C | 5 | H | 5 | W | 125 | 127 | 39.05 | 3.22 | 42.27 | 42.268 | 41.744 | 17.77 | 0.303 | 0.636 |
| 865 | C | 5 | H | 5 | W | 135 | 137 | 39.15 | 3.22 | 42.37 | 42.362 | 41.762 | 12.60 | 0.236 | 0.710 |
| 865 | C | 5 | H | 5 | W | 145 | 147 | 39.25 | 3.22 | 42.47 | 42.456 | 41.781 | 17.73 | 0.271 | 0.654 |
| 865 | C | 5 | H | 6 | W | 5 | 7 | 39.35 | 3.22 | 42.57 | 42.549 | 41.799 | 11.00 | 0.218 | 0.635 |
| 865 | C | 5 | H | 6 | W | 15 | 17 | 39.45 | 3.22 | 42.67 | 42.643 | 41.817 | 18.24 | 0.271 | 0.598 |
| 865 | C | 5 | H | 6 | W | 25 | 27 | 39.55 | 3.22 | 42.77 | 42.737 | 41.836 | 13.01 | 0.194 | 0.571 |
| 865 | C | 5 | H | 6 | W | 35 | 37 | 39.65 | 3.22 | 42.87 | 42.831 | 41.854 | 17.63 | 0.164 | 0.477 |
| 865 | C | 5 | H | 6 | W | 45 | 47 | 39.75 | 3.22 | 42.97 | 42.924 | 41.873 | 12.46 | 0.114 | 0.472 |
| 865 | C | 5 | H | 6 | W | 55 | 57 | 39.85 | 3.22 | 43.07 | 43.018 | 41.891 | 12.88 | 0.217 | 0.569 |
| 865 | C | 5 | H | 6 | W | 65 | 67 | 39.95 | 3.22 | 43.17 | 43.112 | 41.909 | 8.59 | 0.160 | 0.440 |
| 865 | C | 5 | H | 6 | W | 70 | 72 | 40.01 | 3.22 | 43.23 | 43.168 | 41.920 | - | -0.081 | 0.312 |
| 865 | C | 5 | H | 6 | W | 75 | 77 | 40.05 | 3.22 | 43.27 | 43.206 | 41.928 | 14.49 | 0.130 | 0.390 |
| 865 | C | 5 | H | 6 | W | 85 | 87 | 40.15 | 3.22 | 43.37 | 43.299 | 41.946 | 13.46 | 0.166 | 0.478 |
| 865 | C | 5 | H | 6 | W | 95 | 97 | 40.25 | 3.22 | 43.47 | 43.393 | 41.964 | 15.21 | 0.249 | 0.450 |
| 865 | C | 5 | H | CC | W | 20 | 22 | 40.54 | 3.22 | 43.76 | 43.665 | 42.018 | 10.23 | 0.146 | 0.455 |
| 865 | C | 6 | H | 1 | W | 15 | 17 | 41.45 | 3.46 | 44.91 | 44.950 | 42.265 | 12.25 | 0.349 | 0.523 |
| 865 | C | 6 | H | 1 | W | 35 | 37 | 41.65 | 3.46 | 45.11 | 45.165 | 42.306 | 13.16 | 0.253 | 0.484 |
| 865 | C | 6 | H | 1 | W | 55 | 57 | 41.85 | 3.46 | 45.31 | 45.347 | 42.340 | 14.44 | 0.394 | 0.789 |

| | | | | | | | | | | | | | | | |
|---|---|---|---|---|---|---|---|---|---|---|---|---|---|---|---|
| 865 | C | 6 | H | 1 | W | 75 | 77 | 42.05 | 3.46 | 45.51 | 45.529 | 42.375 | 11.53 | 0.244 | 0.548 |
| 865 | C | 6 | H | 1 | W | 95 | 97 | 42.25 | 3.46 | 45.71 | 45.711 | 42.409 | 11.96 | 0.366 | 0.727 |
| 865 | C | 6 | H | 1 | W | 115 | 117 | 42.45 | 3.46 | 45.91 | 45.910 | 42.447 | 10.64 | 0.264 | 0.513 |
| 865 | C | 6 | H | 1 | W | 135 | 137 | 42.65 | 3.46 | 46.11 | 46.110 | 42.485 | 15.75 | 0.365 | 0.691 |
| 865 | C | 6 | H | 2 | W | 5 | 7 | 42.85 | 3.46 | 46.31 | 46.310 | | 10.40 | 0.285 | 0.612 |
| 865 | C | 6 | H | 2 | W | 25 | 27 | 43.05 | 3.46 | 46.51 | 46.510 | | 13.11 | -0.062 | 0.493 |
| 865 | C | 6 | H | 2 | W | 45 | 47 | 43.25 | 3.46 | 46.71 | 46.710 | | 14.32 | 0.206 | 0.709 |
| 865 | C | 6 | H | 2 | W | 63 | 65 | 43.43 | 3.46 | 46.89 | 46.890 | | 14.44 | 0.293 | 0.785 |
| 865 | C | 6 | H | 2 | W | 125 | 127 | 44.05 | 3.46 | 47.51 | 47.510 | | 12.72 | 0.195 | 0.760 |

NB. Samples with no coarse fraction data are shipboard samples

**Supplementary Table 5. Tuning tie-points**

| 405 kyr minima in La2011 | Depth of ln Sr/Ca filtered maxima (amcd) | Sedimentation rate (cm/kyr) |
|---|---|---|
| 37.255 | | |
| 37.657 | 22.86 | |
| 38.07 | 24.72 | 0.450 |
| 38.466 | 26.68 | 0.495 |
| 38.871 | 28.26 | 0.390 |
| 39.278 | 30.04 | 0.437 |
| 39.674 | 32.14 | 0.530 |
| 40.076 | 34.24 | 0.522 |
| 40.47 | 36.54 | 0.584 |
| 40.879 | 38.46 | 0.469 |
| 41.289 | 40.26 | 0.439 |
| 41.703 | 42.06 | 0.435 |
| 42.107 | 44.12 | 0.510 |
| 42.506 | 46.22 | 0.526 |
| 42.912 | | |